

WoodFisher: Efficient second-order approximations for model compression

SIDAK PAL SINGH¹
contact@sidakpal.com

and

DAN ALISTARH²
dan.alistarh@ist.ac.at

¹EPFL & IST Austria

²IST Austria

April 6, 2020

Work done as part of the first author's master thesis requirement at EPFL.

Abstract

Second-order information, in the form of Hessian- or Inverse-Hessian-vector products, is a fundamental tool for solving optimization problems. Recently, there has been a tremendous amount of work on utilizing this information for the current compute and memory-intensive deep neural networks, usually via coarse-grained approximations (such as diagonal, block-wise, or Kronecker-factorization).

However, not much is known about the quality of these approximations. Our work addresses this question, and in particular, we propose a method called ‘WoodFisher’ that leverages the structure of the empirical Fisher information matrix, along with the Woodbury matrix identity, to compute a faithful and efficient estimate of the inverse Hessian.

Our main application is to the task of compressing neural networks, where we build on the classical Optimal Brain Damage/Surgeon framework (LeCun et al., 1990; Hassibi and Stork, 1993). We demonstrate that WoodFisher significantly outperforms magnitude pruning (isotropic Hessian), as well as methods that maintain other diagonal estimates. Further, even when gradual pruning is considered, our method results in a gain in test accuracy over the state-of-the-art approaches, for standard image classification datasets such as CIFAR-10, ImageNet. We also propose a variant called ‘WoodTaylor’, which takes into account the first-order gradient term, and can lead to additional improvements. An important advantage of our methods is that they allow us to automatically set the layer-wise pruning thresholds, avoiding the need for any manual tuning or sensitivity analysis.

Contents

Abstract	i
1 Introduction	1
1.1 Formal Setup	3
1.2 Neural Networks	3
1.3 Local quadratic model	4
1.4 Probabilistic view	5
1.5 Fisher Information Matrix	7
1.6 Gauss-Newton Matrix	8
1.7 Empirical Fisher	9
2 Model Compression	11
2.1 Problem Formulation	11
2.2 Pruning at local optimum	12
2.2.1 Removing a single parameter w_q	13
2.2.2 Removing multiple parameters at once	14
2.2.3 Cases for specific kinds of Hessian	16
2.3 Related Work	16
3 Efficient IHVP approximation	19
3.1 A visual exploration of Hessian and empirical Fisher matrices	19
3.1.1 On MNIST	19
3.1.2 On CIFAR10	21
3.2 Inverting the empirical Fisher	23
3.3 Approximation quality of the local quadratic model	25
3.4 Discussion	26
3.4.1 Suitability of the Empirical Fisher	26
3.4.2 Issues with using K-FAC	27
3.5 Other approximation methods	30
4 Experiments	33
4.1 One-shot pruning results	34
4.1.1 On MNIST	34
4.1.2 On CIFAR10	35

Contents

4.1.3 On ImageNet	36
4.2 Ablation studies	37
4.3 Gradual pruning results	38
4.4 Comparison with state-of-the-art methods	40
5 Extensions	43
5.1 WoodTaylor: Pruning at a general point	43
5.2 Empirical Results	45
5.2.1 Partially trained model	45
5.2.2 Pre-trained model	46
6 Conclusion and Future Work	49
Bibliography	51

1 Introduction

With the recent success of deep learning, e.g. (LeCun et al., 2015; Schmidhuber, 2015), we are witnessing an unprecedented accuracy improvement on a range of tasks in computer vision (Ren et al., 2015; He et al., 2016) or natural language processing (Devlin et al., 2018; Radford, 2018). Central to this performance progression has been the size of the underlying models, with millions and billions of trainable parameters (He et al., 2016; Devlin et al., 2018). This trend seems unlikely to cease, with industrial research labs inching towards training a *trillion* parameter model (Rajbhandari et al., 2019).

This general trend of training and deploying large models is taxing from the performance perspective. In turn, it has resulted in another line of work, where researchers compress such parameter-heavy deep neural networks into “lighter,” easier to deploy variants. This challenge is not new, and in fact, results in this direction can be found as early as the 1990s. Thus, most of the recent work to tackle this challenge can in fact find its roots in these classic previous works. This paper investigates the compression of deep neural models, and finds inspiration from the work on Optimal Brain Damage/Surgeon (OBD/OBS) (LeCun et al., 1990; Hassibi and Stork, 1993). The main idea behind this framework is to build a local quadratic model approximation based on the second-order Taylor series expansion to optimally determine the parameters to be removed. We describe it precisely in Chapter 2.

Applying second-order methods, at the scale of model sizes described above, might sound odd. While there has been a tremendous amount of work on utilizing the second-order information for deep networks—usually via coarse-grained approximations (such as diagonal, or block-wise, or Kronecker-factorization)—little is known about their quality and scalability. In our work, we address the former question in detail in Chapter 3, and show how the empirical Fisher information matrix used alongside the Woodbury matrix identity can provide an estimate of inverse-Hessian-vector products (IHVPs), which is efficient and yet faithfully represents the structure contained in the Hessian.

To address the question of scalability and practicality, we demonstrate in Chapter 4, how our method for estimating IHVPs can be used in conjunction with OBD/OBS framework, resulting

Chapter 1. Introduction

in a state-of-the-art one-shot pruner for various commonly used networks such as ResNet-20, ResNet-50 (He et al., 2016) on standard image-classification dataset like CIFAR-10 and ImageNet. Even when intermediate re-training is allowed, as in the case of gradual pruning, our method performs at par if not better than state-of-the-art pruning approaches, including dynamic pruning methods. We also propose an extension in Chapter 5 which takes into account the often-dropped gradient term in the local quadratic model and show that it leads to a further performance gain.

To conclude, it is of paramount importance that we understand more about the theoretical underpinnings of neural networks, as sooner or later we will reach the limits of computation and today's dominant approach of scaling things up would not last. Although model compression on its own is unlikely to provide a complete picture of this phenomenon, the insights about which parameters to keep and which to prune will potentially be a vital tool in enabling us to train neural networks of the right size from the outset. We hope that our method to efficiently estimate inverse-Hessian-vector products will serve as a first step in this direction.

1.1 Formal Setup

In supervised machine learning, we generally assume the following setup. We are given a set S of training examples, each of which is composed of an input $\mathbf{x} \in \mathcal{X}$ and corresponding output $\mathbf{y} \in \mathcal{Y}$. The goal is to learn a mapping $f: \mathcal{X} \rightarrow \mathcal{Y}$ such that given input \mathbf{x} , the prediction $f(\mathbf{x}; \mathbf{w})$ is close to the underlying output \mathbf{y} . Generally, we take $\mathcal{X} = \mathbb{R}^m$ and $\mathcal{Y} = \mathbb{R}^k$, where m and k denote the dimensionality of the input and the output respectively. We consider that our function (or mapping) f has parameters (or weights) $\mathbf{w} \in \mathbb{R}^d$, and learning then corresponds to finding a setting of these parameters which minimizes an objective function.

To formalize this notion, we assume a loss function $\ell: \mathcal{Y} \times \mathcal{Y} \rightarrow \mathbb{R}$ that measures how far is the prediction of our function away from the true output (or target). Hence, we can formulate the objective as an average of this loss over the set of training examples (i.e., the training set),

$$L(\mathbf{w}) = \frac{1}{N} \sum_{n=1}^N \ell(\mathbf{y}_n, f(\mathbf{x}_n; \mathbf{w})). \quad (1.1)$$

The optimal weight value \mathbf{w}^* , is just the $\operatorname{argmin}_{\mathbf{w} \in \mathbb{R}^d} L(\mathbf{w})$. This optimization problem is typically solved via a first-order method like gradient descent. Essentially, this means that at each step in the optimization procedure, we move in the direction of the negative gradient of the overall function $L(\mathbf{w})$ from Eq. (1.1), scaled by the learning rate η . Therefore we have,

$$\mathbf{w}_{t+1} := \mathbf{w}_t - \eta \nabla L(\mathbf{w}_t). \quad (1.2)$$

1.2 Neural Networks

The choice for the class of functions that we consider in this work is neural networks, in view of the massive success of deep learning (LeCun et al., 2015; Schmidhuber, 2015). While our discussion here will focus on fully-connected and convolutional neural networks (CNNs), our work applies equally to the other kinds of networks, such as recurrent neural networks (RNNs).

Neural networks, at their core, are a sequence of affine transformations composed with non-linear activations. Let us say that the neural network under consideration has l layers. Then, the output activation \mathbf{a}_i of the i^{th} layer is given as, $\mathbf{a}_i = \sigma(W_i \mathbf{a}_{i-1} + \mathbf{b}_i)$, while \mathbf{a}_0 is defined to be equal to the input \mathbf{x} . Also, here σ denotes the non-linear activation function (such as ReLU or Sigmoid), W_i and \mathbf{b}_i are the weight matrix and bias parameters corresponding to layer i . The overall output of the neural network can then be written as $f(\mathbf{x}; \mathbf{w}) = \mathbf{a}_l$.

Note that, as a shorthand, we are denoting all the parameters $\{(W_i, \mathbf{b}_i)_{i=1}^l\}$ together by \mathbf{w} . Further, for the sake of brevity, we will exclude the bias parameters in the discussion hereafter. However, the same arguments apply to them without loss of generality.

1.3 Local quadratic model

If we look back at the weight update in Eq. (1.2), this can be viewed as the solution to a sub-problem, where we linearize our function L at \mathbf{w}_t and look for an update $\delta\mathbf{w}$ that minimizes the function value at $\mathbf{w}_{t+1} = \mathbf{w}_t + \delta\mathbf{w}$, but subject to a penalty on how far we go from \mathbf{w}_t (or how big our update $\delta\mathbf{w}$ can be). Mathematically, this can be described as,

$$\min_{\delta\mathbf{w} \in \mathbb{R}^d} \left\{ L(\mathbf{w}_t) + \nabla L(\mathbf{w}_t)^\top \delta\mathbf{w} + \frac{1}{2\eta} \|\delta\mathbf{w}\|^2 \right\}. \quad (1.3)$$

This results in the weight update $\delta\mathbf{w} = -\eta \nabla L(\mathbf{w}_t)$.

Newton step. Note that, in the above equation we measure the size of our step/update in the Euclidean norm. A more natural choice is to consider the norm with respect to the Hessian matrix \mathbf{H} , which to recall is defined as follows (for a twice-differentiable function),

$$\mathbf{H} = \nabla_{\mathbf{w}}^2 L = \begin{pmatrix} \frac{\partial^2 L}{\partial w_1 \partial w_1} & \frac{\partial^2 L}{\partial w_1 \partial w_2} & \cdots & \frac{\partial^2 L}{\partial w_1 \partial w_d} \\ \frac{\partial^2 L}{\partial w_2 \partial w_1} & \frac{\partial^2 L}{\partial w_2 \partial w_2} & \cdots & \frac{\partial^2 L}{\partial w_2 \partial w_d} \\ \vdots & \vdots & \cdots & \vdots \\ \frac{\partial^2 L}{\partial w_d \partial w_1} & \frac{\partial^2 L}{\partial w_d \partial w_2} & \cdots & \frac{\partial^2 L}{\partial w_d \partial w_d} \end{pmatrix}. \quad (1.4)$$

Importantly, the Hessian allows us to account for the local geometry of the function L at a given point w . Thus we can instead consider a similar problem to that given in Eq. (1.3), but with respect to the norm measured by the Hessian.

$$\min_{\delta\mathbf{w} \in \mathbb{R}^d} \left\{ L(\mathbf{w}_t) + \nabla L(\mathbf{w}_t)^\top \delta\mathbf{w} + \frac{1}{2} \delta\mathbf{w}^\top \mathbf{H} \delta\mathbf{w} \right\}. \quad (1.5)$$

The resulting update is called the Newton step, $\delta\mathbf{w} = -\mathbf{H}^{-1} \nabla L(\mathbf{w}_t)$, and the optimization procedure is referred to as Newton's method. An alternative way to look at this is by considering the second-order Taylor series expansion at \mathbf{w}_t for a small update $\delta\mathbf{w}$, such that the higher-order terms vanish. This approximation for the loss in the neighbourhood of \mathbf{w}_t is what is known as the local quadratic model.

Advantage over first-order methods. For convex functions, it is known that gradient descent converges to the global optimum at a linear rate¹, under additional assumptions of smoothness and strong-convexity. The advantage of Newton's method is that it achieves a much faster (local) quadratic rate of convergence under some technical assumptions on the

¹Linear convergence means that to reach an error ε , it requires $\mathcal{O}(\log(1/\varepsilon))$ steps. Quadratic rate on the other hand means $\mathcal{O}(\log \log(1/\varepsilon))$ steps.

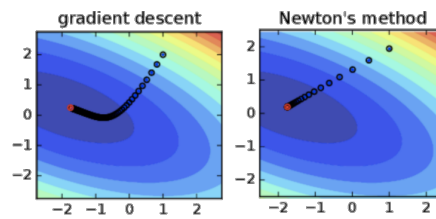


Figure 1.1 – Behaviour of gradient descent and Newton’s method for a quadratic function. Image source: <http://tiny.cc/4bwemz>.

Hessian. Thus, Hessians form a fundamental tool in optimization.

To illustrate this visually, in Figure 1.1, we consider the example of a quadratic function and compare the behaviour of gradient descent versus Newton’s method. Here, the update from the Newton step has also been scaled by the learning rate η . We see that gradient descent requires significantly more iterations to converge in comparison to Newton’s method which adapting to the curvature goes straight to the minimum.

Challenges for application in deep learning. However, when applied to the setting of neural networks, the objective function is highly non-convex. This implies that the Hessian need not be positive semi-definite, as in the case of convex functions. As a result, the Hessian might not be easy to invert (or can be non-invertible at all).

Another problem surrounding the use of the Newton step is its high computational cost. Contemporary neural-networks have millions of parameters, say ResNet-50 (He et al., 2016), if not more. Thus, building the full Hessian and inverting is simply out of the question. Therefore, while the number of iterations for Newton’s method might be more, each step can be much more computationally expensive. We discuss these aspects in more detail in the related work section 3.5.

1.4 Probabilistic view

In this section, we consider the supervised learning framework from a probabilistic perspective. We closely follow Martens (2014) for this section of the background.

First, we assume that there is an underlying joint distribution $Q_{\mathbf{x},\mathbf{y}}$ that describes the training data. This can be factorized as, $Q_{\mathbf{x},\mathbf{y}} = Q_{\mathbf{x}} Q_{\mathbf{y}|\mathbf{x}}$. The first quantity denotes the distribution from which the inputs are sampled, while the second describes the conditional distribution of the output \mathbf{y} given the input \mathbf{x} . In general, since our task is concerned with predicting the output given input, we are interested in modelling and learning this conditional distribution. The marginal distribution $Q_{\mathbf{x}}$ is also reflected by the inputs in the training set, and in practice, is estimated by the empirical distribution $\hat{Q}_{\mathbf{x}}$.

Chapter 1. Introduction

Thus, we can view the training of a neural network as learning a conditional distribution, $P_{\mathbf{y}|\mathbf{x}}$, which is close to the true $Q_{\mathbf{y}|\mathbf{x}}$. Note that, the model's conditional distribution depends on the parameters \mathbf{w} and writing it as $P_{\mathbf{y}|\mathbf{x}}(\mathbf{w})$ is more accurate. However, we will skip this distinction in our notations unless required. The joint distribution given by the neural network can be expressed as, $P_{\mathbf{x},\mathbf{y}} = Q_{\mathbf{x}}P_{\mathbf{y}|\mathbf{x}}$.

Hence, let us re-formulate our learning objective as minimizing the Kullback-Leibler (KL) divergence between the two joint distributions.

$$\text{KL}(Q_{\mathbf{x},\mathbf{y}}\|P_{\mathbf{x},\mathbf{y}}) = \int q(\mathbf{x},\mathbf{y}) \log \frac{q(\mathbf{x},\mathbf{y})}{p_{\mathbf{w}}(\mathbf{x},\mathbf{y})} d\mathbf{x} d\mathbf{y}, \quad (1.6)$$

where $q(\mathbf{x},\mathbf{y})$ and $p_{\mathbf{w}}(\mathbf{x},\mathbf{y})$ denote the joint density function corresponding to the distributions Q and P respectively. By using the above-mentioned factorization of these distributions, we can further rewrite Eq.(1.6) as follows:

$$\begin{aligned} \text{KL}(Q_{\mathbf{x},\mathbf{y}}\|P_{\mathbf{x},\mathbf{y}}) &= \int q(\mathbf{x})q(\mathbf{y}|\mathbf{x}) \log \frac{q(\mathbf{x})q(\mathbf{y}|\mathbf{x})}{q(\mathbf{x})p_{\mathbf{w}}(\mathbf{y}|\mathbf{x})} d\mathbf{x} d\mathbf{y} \\ &= \int q(\mathbf{x}) \int q(\mathbf{y}|\mathbf{x}) \log \frac{q(\mathbf{y}|\mathbf{x})}{p_{\mathbf{w}}(\mathbf{y}|\mathbf{x})} d\mathbf{y} d\mathbf{x} \\ &= \int q(\mathbf{x}) \text{KL}(Q_{\mathbf{y}|\mathbf{x}}\|P_{\mathbf{y}|\mathbf{x}}) d\mathbf{x} \\ &= E_{Q_{\mathbf{x}}} [\text{KL}(Q_{\mathbf{y}|\mathbf{x}}\|P_{\mathbf{y}|\mathbf{x}})] \\ &\stackrel{(a)}{\approx} \frac{1}{N} \sum_{n=1}^N \text{KL}(Q_{\mathbf{y}|\mathbf{x}_n}\|P_{\mathbf{y}|\mathbf{x}_n}) \\ &\stackrel{(b)}{=} \frac{1}{N} \sum_{n=1}^N \mathbb{1} \log \frac{1}{p_{\mathbf{w}}(\mathbf{y}_n|\mathbf{x}_n)} = -\frac{1}{N} \sum_{n=1}^N \log(p(\mathbf{y}_n|\mathbf{x}_n; \mathbf{w})) \end{aligned} \quad (1.7)$$

The approximation labelled (a) follows if we estimate the marginal distribution $\hat{Q}_{\mathbf{x}}$ by the samples from the empirical training distribution, thus obtaining an average over the training points \mathbf{x}_n instead of the expectation. Next, the equality labelled (b) comes from using the empirical the $\hat{Q}_{\mathbf{y}|\mathbf{x}_n}$ and the fact that it is typically in a one-hot form. For example, in classification, we only have a single label for an input². Lastly, these sets of equations (1.7) can also be interpreted from a maximum likelihood viewpoint.

While we have loosely stated that our neural-network models the conditional distribution $P_{\mathbf{y}|\mathbf{x}}$, this can be made more precise as follows. We consider an auxiliary conditional distribution (also called predictive distribution) $R_{\mathbf{y}|f(\mathbf{x};\mathbf{w})}$ defined on the (deterministic) outputs of the neural network, such that $P_{\mathbf{y}|\mathbf{x}} = R_{\mathbf{y}|f(\mathbf{x};\mathbf{w})}$. The resulting objective of the Eqns. (1.7) can be then

²Although nowadays, with the use of the teacher network to model the true conditional distribution like in Distillation (Hinton et al., 2015), we would have a full expression of the KL.

written as,

$$-\frac{1}{N} \sum_{n=1}^N \log \left(r(\mathbf{y}_n | f(\mathbf{x}_n; \mathbf{w})) \right), \quad (1.8)$$

where, r is the density function corresponding to $R_{\mathbf{y}|f(\mathbf{x};\mathbf{w})}$.

Now, comparing Eq. (1.1) and Eq. (1.8), we can establish their equivalence by the relation,

$$\ell(\mathbf{y}_n, f(\mathbf{x}_n; \mathbf{w})) = -\log(p_{\mathbf{w}}(\mathbf{y}_n | \mathbf{x}_n)) = -\log(r(\mathbf{y}_n | f(\mathbf{x}_n; \mathbf{w}))). \quad (1.9)$$

To give a better idea of the probabilistic perspective of the loss function, consider these two examples:

- If R is a Gaussian distribution, $\mathcal{N}(\mathbf{y}; f, \sigma^2)$, for some constant variance σ^2 , the resulting loss is equivalent to the mean-squared loss.
- Otherwise, if the conditional distribution R on the output corresponds to something like, $r(\mathbf{y}_n = c | f(\mathbf{x}_n; \mathbf{w})) = \frac{\exp(f(\mathbf{x}_n; \mathbf{w})_c)}{\sum_{j=1}^k \exp(f(\mathbf{x}_n; \mathbf{w})_j)}$, then it is the same as performing softmax on the network output composed together with negative log-likelihood loss used in k -class classification problem.

1.5 Fisher Information Matrix

Under the probabilistic framework of the previous section, we can define something called the Fisher information matrix F of the model's conditional distribution $P_{\mathbf{y}|\mathbf{x}}$ as follows,

$$F = E_{P_{\mathbf{x},\mathbf{y}}} \left[\nabla_{\mathbf{w}} \log p_{\mathbf{w}}(\mathbf{x}, \mathbf{y}) \nabla_{\mathbf{w}} \log p_{\mathbf{w}}(\mathbf{x}, \mathbf{y})^{\top} \right]. \quad (1.10)$$

In fact, it can be proved that Fisher is also equal to the expectation of the following quantity,

$$F = E_{P_{\mathbf{x},\mathbf{y}}} \left[-\nabla_{\mathbf{w}}^2 \log p_{\mathbf{w}}(\mathbf{x}, \mathbf{y}) \right]. \quad (1.11)$$

We refer the readers to [Kunstner et al. \(2019\)](#) for this proof and a nice exposition about the topic. Next, this term inside the expectation is the Hessian of the loss ℓ at (\mathbf{x}, \mathbf{y}) in Eq. (1.9). In fact, we show further that the Fisher information matrix defined in Eq. (1.10) and Hessian matrix in Eq. (1.4) are equivalent *when the model and data distribution match*. But before going ahead, we note that we will drop the subscript \mathbf{w} under the gradient and the Hessian terms to simplify the notation.

First, we factorize the model's joint distribution as before, and estimate the marginal $Q_{\mathbf{x}}$ by its empirical version $\hat{Q}_{\mathbf{x}}$. In other words, we have that $P_{\mathbf{y},\mathbf{x}} = Q_{\mathbf{x}} P_{\mathbf{y}|\mathbf{x}} \approx \hat{Q}_{\mathbf{x}} P_{\mathbf{y}|\mathbf{x}}$. Then using this, we

can write the Fisher as follows,

$$F = \frac{1}{N} \sum_{n=1}^N E_{P_{\mathbf{y}|\mathbf{x}_n}} \left[\nabla \log p_{\mathbf{w}}(\mathbf{y}|\mathbf{x}_n) \nabla \log p_{\mathbf{w}}(\mathbf{y}|\mathbf{x}_n)^\top \right] = \frac{1}{N} \sum_{n=1}^N E_{P_{\mathbf{y}|\mathbf{x}_n}} \left[-\nabla^2 \log p_{\mathbf{w}}(\mathbf{y}|\mathbf{x}_n) \right] \quad (1.12)$$

Then if the model's conditional distribution $P_{\mathbf{y}|\mathbf{x}}$ matches the conditional distribution of the data $\hat{Q}_{\mathbf{y}|\mathbf{x}}$, we obtain,

$$\begin{aligned} F &= \frac{1}{N} \sum_{n=1}^N E_{\hat{Q}_{\mathbf{y}|\mathbf{x}_n}} \left[-\nabla^2 \log p_{\mathbf{w}}(\mathbf{y}|\mathbf{x}_n) \right] \\ &= \frac{1}{N} \sum_{n=1}^N -\nabla^2 \log p_{\mathbf{w}}(\mathbf{y}_n|\mathbf{x}_n) \\ &\stackrel{(1.9)}{=} \frac{1}{N} \sum_{n=1}^N -\nabla^2 \log p_{\mathbf{w}}(\mathbf{y}_n|\mathbf{x}_n) \\ &\stackrel{(1.1)}{=} \frac{1}{N} \sum_{n=1}^N \nabla^2 \ell(\mathbf{y}_n|f(\mathbf{x}_n; \mathbf{w})) = \mathbf{H}. \end{aligned} \quad (1.13)$$

Therefore, we conclude that under the assumption where the model and data distribution match, Fisher and Hessian matrices are equivalent.

This implies that we can consider an alternative variant of the Newton step which uses the inverse of the Fisher instead of the Hessian. As a matter of fact, [Amari \(1998\)](#) has proposed such a usage of the Fisher in the well-known '*Natural Gradient*', which is albeit motivated from the different perspective of adapting to the model's information geometry. The natural gradient can essentially be derived by measuring the change in parameters in terms of the KL-divergence, similar to the sub-problems in Eqns (1.3) and (1.5), where we used the Euclidean distance and the metric given by the Hessian to obtain the updates for gradient descent and Newton's step respectively.

1.6 Gauss-Newton Matrix

In this section, we discuss another approach that sheds light on the close relationship between the Fisher and the Hessian. Consider, we have the following least-squares objective,

$$L(\mathbf{w}) = \frac{1}{2N} \sum_n (f(\mathbf{x}_n; \mathbf{w}) - \mathbf{y}_n)^2. \quad (1.14)$$

The analytical expression of the Hessian is then given by,

$$\mathbf{H} = \nabla^2 L(\mathbf{w}) = \underbrace{\frac{1}{N} \sum_n \nabla f(\mathbf{x}_n; \mathbf{w}) \nabla f(\mathbf{x}_n, \mathbf{w})^\top}_{:=G(\mathbf{w})} + \underbrace{\frac{1}{N} \sum_n r_n \nabla^2 f(\mathbf{x}_n, \mathbf{w})}_{:=R(\mathbf{w})}. \quad (1.15)$$

where, $r_n = f(x_n, w) - y_n$, denote the residuals. The first term $G(\mathbf{w})$ is called the Gauss-Newton matrix. As the residuals get smaller, we see that the second term approaches zero, and the Gauss-Newton matrix becomes a good approximation to the Hessian. When there is a perfect fit, or in probabilistic parlance, when the model and data distributions match, we have that the Gauss-Newton is exactly equal to the Hessian matrix. In such a scenario, we thus obtain that the Hessian, Fisher, and Gauss-Newton matrices are equivalent.

While here we discussed only the least-squares objective, such a result has been generalized to hold true by [Schraudolph \(2002\)](#) in the case of other loss functions (which are convex in the output of the network), like the cross-entropy loss used often in classification.

If we denote the Jacobian of the network outputs $f(\mathbf{x}_n, \mathbf{w})$ with respect to the parameters \mathbf{w} by $J_n = J_{\mathbf{w}} f(\mathbf{x}_n; \mathbf{w})$, and the Hessian of the loss function ℓ with respect to the network output f by \mathbf{H}_ℓ , we can write the Generalized-Gauss-Newton (GGN) matrix as follows,

$$G(\mathbf{w}) = \frac{1}{N} \sum_n J_n^\top \mathbf{H}_\ell J_n. \quad (1.16)$$

Note, the obtained Gauss-Newton matrix for the least-squares objective is a special case of this, since for least-squares H_ℓ is equal to the identity matrix.

Further, when the predictive distribution $R_{\mathbf{y}|f(\mathbf{x}; \mathbf{w})}$ is a distribution from an exponential family, we can write Fisher without expectations ([Martens \(2014\)](#), Section 9.2). Basically, this is due to the fact that $\nabla_f^2 [-\log p_{\mathbf{w}}(\mathbf{y}|\mathbf{x})]$ is independent of the sampled \mathbf{y} for an exponential family. In such a case, the Fisher matches the Gauss-Newton and is equivalent to the formulation expressed in Eqn. (1.16).

1.7 Empirical Fisher

Now, we talk about the one last concept that will be introduced in the background here, namely the empirical Fisher \hat{F} .

This matrix is an approximation to the Fisher matrix introduced in Eq. (1.10), where we replace the model distribution $P_{\mathbf{x}, \mathbf{y}}$ with the empirical training distribution $\hat{Q}_{\mathbf{x}, \mathbf{y}}$. Thus we can simplify

the expression of empirical Fisher as follows,

$$\begin{aligned}\hat{F} &= E_{\hat{Q}_{\mathbf{x}, \mathbf{y}}} [\nabla \log p_{\mathbf{w}}(\mathbf{x}, \mathbf{y}) \nabla \log p_{\mathbf{w}}(\mathbf{x}, \mathbf{y})^\top] \\ &= E_{\hat{Q}_{\mathbf{x}}} \left[E_{\hat{Q}_{\mathbf{y}|\mathbf{x}}} [\nabla \log p_{\mathbf{w}}(\mathbf{y}|\mathbf{x}) \nabla \log p_{\mathbf{w}}(\mathbf{y}|\mathbf{x})^\top] \right] \\ &= \frac{1}{N} \sum_{n=1}^N \nabla \log p(\mathbf{y}_n | f(\mathbf{x}_n; \mathbf{w})) \nabla \log p(\mathbf{y}_n | f(\mathbf{x}_n; \mathbf{w}))^\top.\end{aligned}\tag{1.17}$$

By using the equivalence of the loss presented before in Eq. (1.9), we can further rewrite the above expression as,

$$\hat{F} = \frac{1}{N} \sum_{n=1}^N \nabla \ell(\mathbf{y}_n, f(\mathbf{x}_n; \mathbf{w})) \nabla \ell(\mathbf{y}_n, f(\mathbf{x}_n; \mathbf{w}))^\top = \frac{1}{N} \sum_{n=1}^N \nabla \ell_n \nabla \ell_n^\top,\tag{1.18}$$

where, in the last step, we have used a shorthand ℓ_n to denote the loss for a particular training example $(\mathbf{x}_n, \mathbf{y}_n)$.

2 Model Compression

As alluded to in the introduction, with the recent success of deep learning on various applications tasks in natural language ([Devlin et al., 2018](#)) and vision ([He et al., 2016](#)), we are faced with an interesting problem. A lot of these advancements also inherently involve increased model capacity, and that too by a significant factor. This raises the question of how do we actually employ these networks in practice, to really gain from these advancements, besides just better performance on the benchmark datasets.

The above problem that we are facing is however not new, and in fact, such methods to compress models had their history before the last neural-network winter of the '90s ([Mozer and Smolensky, 1989](#); [LeCun et al., 1990](#); [Hassibi and Stork, 1993](#)). In this section, we follow the classical works of Optimal Brain Damage/Surgeon proposed in [LeCun et al. \(1990\)](#); [Hassibi and Stork \(1993\)](#) and elaborate the underlying framework.

2.1 Problem Formulation

We assume that we are given a neural network which has been trained to convergence. This network typically has a huge number of parameters, in the order of millions. In this over-parameterized regime, we can expect that there exists a neural network within the given large neural network, which has fewer parameters but still achieves similar performance in comparison to the latter ([Frankle and Carbin, 2018](#)).

While ideally, we would want to simply train a neural network of the right size from the outset, this is harder than it seems. So currently, we just focus on pruning (or removing) the parameters from the given large neural network. In fact, this route of obtaining compact neural networks might still be needed to compress pre-trained networks that are already available and need to be deployed, say at an edge device.

Further, we will look at the setting of unstructured pruning, where individual weights and biases of the network are removed at a time, rather than deleting all parameters of a neuron at once (as in structured pruning). In a way, unstructured pruning is more general than

structured pruning since all the parameters of a neuron might eventually get removed.

Hence, in other words, the goal here with pruning is to modify the current parameters of our neural network in a way that sets more of them to zero, while maintaining the performance. We use the training loss to measure the performance, and would like the change in training loss to be minimal after such a modification of the parameters.

Let us denote all the parameters of neural network by the vector \mathbf{w} , so as to analyse the effect of pruning at a more generic level, without distinguishing between weights and biases. Next, let $\delta\mathbf{w}$ denote this perturbation we apply to our parameters. The training loss is denoted by $L: \mathbb{R}^d \mapsto \mathbb{R}$ where d is the dimensionality or size of parameters \mathbf{w} , and is typically given by:

$$L(\mathbf{w}) = \frac{1}{N} \sum_{i=1}^N \ell(y_i, f(\mathbf{x}_i; \mathbf{w})). \quad (2.1)$$

Here, (\mathbf{x}_i, y_i) are samples from the training set S of size N and f denotes the output of the neural network with parameters \mathbf{w} at input \mathbf{x}_i .

Assuming that our update $\delta\mathbf{w}$ to the parameters is small enough, we can use the Taylor series expansion to measure the training loss at the new parameters $\mathbf{w} + \delta\mathbf{w}$. Consider, the second order Taylor series expansion of the function L near \mathbf{w} as follows:

$$L(\mathbf{w} + \delta\mathbf{w}) = L(\mathbf{w}) + \nabla_{\mathbf{w}} L^\top \delta\mathbf{w} + \frac{1}{2} \delta\mathbf{w}^\top \nabla_{\mathbf{w}}^2 L \delta\mathbf{w} + O(\|\delta\mathbf{w}\|^3) \quad (2.2)$$

To simplify notation, let us denote the hessian $\nabla_{\mathbf{w}}^2 L$ by \mathbf{H} and the change in loss $L(\mathbf{w} + \delta\mathbf{w}) - L(\mathbf{w})$ by δL . Therefore, this change in loss can then be approximated as follows:

$$\delta L \approx \nabla_{\mathbf{w}} L^\top \delta\mathbf{w} + \frac{1}{2} \delta\mathbf{w}^\top \mathbf{H} \delta\mathbf{w} \quad (2.3)$$

2.2 Pruning at local optimum

In this section, we assume that network is pruned at (or close to) a local optimum. Hence, we can consider $\nabla_{\mathbf{w}} L = 0$ (or when close to a local optimum, $\nabla_{\mathbf{w}} L \approx 0$) and simplify the expression in Eq. (2.4) to the following:

$$\delta L \approx \frac{1}{2} \delta\mathbf{w}^\top \mathbf{H} \delta\mathbf{w} \quad (2.4)$$

2.2.1 Removing a single parameter w_q

Before proceeding further, we would like to remark that the analysis which factors in the first-order gradient term is considered in the Chapter 5.1 ahead. Now, our goal in pruning is to remove parameters that do not change the loss by a significant amount.

For now, let us consider the case when just a single parameter at index q is removed. The corresponding perturbation $\delta\mathbf{w}$ can be expressed by the constraint $\mathbf{e}_q^\top \delta\mathbf{w} + w_q = 0$, where \mathbf{e}_q denotes the q^{th} canonical basis vector. Then pruning can be formulated as finding the optimal perturbation that satisfies this constraint, and the overall problem can be written as follows:

$$\min_{\delta\mathbf{w} \in \mathbb{R}^d} \left(\frac{1}{2} \delta\mathbf{w}^\top \mathbf{H} \delta\mathbf{w} \right), \quad \text{s.t.} \quad \mathbf{e}_q^\top \delta\mathbf{w} + w_q = 0. \quad (2.5)$$

In order to impose the best choice for the parameter to be removed, we can further consider the following constrained minimization problem.

$$\min_{q \in [d]} \left\{ \min_{\delta\mathbf{w} \in \mathbb{R}^d} \left(\frac{1}{2} \delta\mathbf{w}^\top \mathbf{H} \delta\mathbf{w} \right), \quad \text{s.t.} \quad \mathbf{e}_q^\top \delta\mathbf{w} + w_q = 0 \right\}. \quad (2.6)$$

However, let us first focus on the inner problem, i.e., the one from Eq. (2.5). As this is a constrained optimization problem, we can consider the Lagrange multiplier λ for the constraint and write the Lagrangian $\mathcal{L}(\delta\mathbf{w}, \lambda)$ as follows,

$$\mathcal{L}(\delta\mathbf{w}, \lambda) = \frac{1}{2} \delta\mathbf{w}^\top \mathbf{H} \delta\mathbf{w} + \lambda \left(\mathbf{e}_q^\top \delta\mathbf{w} + w_q \right). \quad (2.7)$$

The lagrange dual function $g(\lambda)$, which is the infimum of the Lagrangian in Eq. (2.7) with respect to \mathbf{w} , can be then obtained by first differentiating Eq. 2.7 and setting it to 0, and then substituting the obtained value of $\delta\mathbf{w}$. These steps are indicated respectively in Eq. (2.8) and Eq. (2.9) below.

$$\mathbf{H} \delta\mathbf{w} + \lambda \mathbf{e}_q = 0 \implies \delta\mathbf{w} = -\lambda \mathbf{H}^{-1} \mathbf{e}_q. \quad (2.8)$$

$$g(\lambda) = \frac{\lambda^2}{2} \mathbf{e}_q^\top \mathbf{H}^{-1} \mathbf{e}_q - \lambda^2 \mathbf{e}_q^\top \mathbf{H}^{-1} \mathbf{e}_q + \lambda w_q = -\frac{\lambda^2}{2} \mathbf{e}_q^\top \mathbf{H}^{-1} \mathbf{e}_q + \lambda w_q. \quad (2.9)$$

Now, maximizing with respect to λ , we obtain that the optimal value λ^* of this lagrange multiplier as

$$\lambda^* = \frac{w_q}{\mathbf{e}_q^\top \mathbf{H}^{-1} \mathbf{e}_q} = \frac{w_q}{[\mathbf{H}^{-1}]_{qq}}. \quad (2.10)$$

The corresponding optimal perturbation, $\delta \mathbf{w}^*$, so obtained is as follows:

$$\delta \mathbf{w}^* = \frac{-w_q \mathbf{H}^{-1} \mathbf{e}_q}{[\mathbf{H}^{-1}]_{qq}}. \quad (2.11)$$

Finally, the resulting change in loss corresponding to the optimal perturbation that removes parameter w_q is,

$$\delta L^* = \frac{w_q^2}{2[\mathbf{H}^{-1}]_{qq}}. \quad (2.12)$$

Going back to the problem in Eq. (2.6), the best choice of q corresponds to removing that parameter w_q which has the minimum value of the above change in loss. We refer to this change in loss as the pruning statistic ρ , see Eq. (2.13), which we compute for all the parameters and then sort them in the descending order of its value.

$$\rho_q = \frac{w_q^2}{2[\mathbf{H}^{-1}]_{qq}}. \quad (2.13)$$

2.2.2 Removing multiple parameters at once

For brevity, consider that we are removing two parameters, q_1 and q_2 , without loss of generality. The constrained optimization corresponding to pruning can be then described as follows,

$$\min_{q_1 \in [d], q_2 \in [d]} \left\{ \min_{\delta \mathbf{w} \in \mathbb{R}^d} \left(\frac{1}{2} \delta \mathbf{w}^\top \mathbf{H} \delta \mathbf{w} \right), \quad \text{s.t.} \quad \mathbf{e}_{q_1}^\top \delta \mathbf{w} + w_{q_1} = 0, \mathbf{e}_{q_2}^\top \delta \mathbf{w} + w_{q_2} = 0, \right\}. \quad (2.14)$$

We can see how the search space for the best parameter choices (q_1, q_2) explodes exponentially. In general, solving this problem optimally seems to be out of hand. Although, it could be possible that the analysis might lead to a tractable computation for the optimal solution. Unfortunately, as described ahead, this is not the case and we will have to resort to some approximation¹ to make things practical.

$$\mathcal{L}(\delta \mathbf{w}, \lambda_1, \lambda_2) = \frac{1}{2} \delta \mathbf{w}^\top \mathbf{H} \delta \mathbf{w} + \lambda_1 \left(\mathbf{e}_{q_1}^\top \delta \mathbf{w} + w_{q_1} \right) + \lambda_2 \left(\mathbf{e}_{q_2}^\top \delta \mathbf{w} + w_{q_2} \right). \quad (2.15)$$

The lagrange dual function² $g'(\lambda_1, \lambda_2)$, which is the infimum of the Lagrangian in Eq. (2.15) with respect to \mathbf{w} , can be then obtained by first differentiating Eq. 2.15 and setting it to 0, and then substituting the obtained value of $\delta \mathbf{w}$. These steps are indicated respectively in Eq. (2.16)

¹Note, we have not even talked about how to obtain (or approximate) the hessian and its inverse efficiently, but that is a story for the next chapter. Stay tuned!

²We denote the lagrange dual function here by g' instead of g to avoid confusion with the notation for lagrange dual function in case of a single multiplier.

and Eq. (2.17) below.

$$\mathbf{H}\delta\mathbf{w} + \lambda_1\mathbf{e}_{q_1} + \lambda_2\mathbf{e}_{q_2} = 0 \implies \delta\mathbf{w} = -\lambda_1\mathbf{H}^{-1}\mathbf{e}_{q_1} - \lambda_2\mathbf{H}^{-1}\mathbf{e}_{q_2}. \quad (2.16)$$

$$g'(\lambda_1, \lambda_2) = -\frac{\lambda_1^2}{2}\mathbf{e}_{q_1}^\top\mathbf{H}^{-1}\mathbf{e}_{q_1} + \lambda_1w_{q_1} - \frac{\lambda_2^2}{2}\mathbf{e}_{q_2}^\top\mathbf{H}^{-1}\mathbf{e}_{q_2} + \lambda_2w_{q_2} - \lambda_1\lambda_2\mathbf{e}_{q_1}^\top\mathbf{H}^{-1}\mathbf{e}_{q_2}. \quad (2.17)$$

Comparing this with the case when a single parameter is removed, c.f. Eq. (2.9), we can rewrite lagrange dual function as follows,

$$g'(\lambda_1, \lambda_2) = g(\lambda_1) + g(\lambda_2) - \lambda_1\lambda_2\mathbf{e}_{q_1}^\top\mathbf{H}^{-1}\mathbf{e}_{q_2}. \quad (2.18)$$

We note that dual function is not exactly separable in terms of the dual variables, λ_1 and λ_2 , unless the off-diagonal term in the hessian inverse corresponding to q_1, q_2 is zero, i.e., $[\mathbf{H}^{-1}]_{q_1q_2} = 0$.

To maximize the dual function in Eq. (2.18) above, we need to solve a linear system with the lagrange multipliers λ_1, λ_2 as variables. The equations for this system program correspond to setting the respect partial derivatives to zero, as described in Eq. (2.19) below,

$$\left. \begin{aligned} \frac{\partial g'}{\partial \lambda_1} &= -\lambda_1\mathbf{e}_{q_1}^\top\mathbf{H}^{-1}\mathbf{e}_{q_1} - \lambda_2\mathbf{e}_{q_1}^\top\mathbf{H}^{-1}\mathbf{e}_{q_2} + w_{q_1} = 0 \\ \frac{\partial g'}{\partial \lambda_2} &= -\lambda_1\mathbf{e}_{q_1}^\top\mathbf{H}^{-1}\mathbf{e}_{q_2} - \lambda_2\mathbf{e}_{q_2}^\top\mathbf{H}^{-1}\mathbf{e}_{q_2} + w_{q_2} = 0 \end{aligned} \right\} \text{Solve to obtain } \lambda_1^*, \lambda_2^* \quad (2.19)$$

Hence, it is evident that exactly solving this resulting linear system will get intractable when we consider the removal of many parameters at once.

Pruning Direction. As a practical approximation to this, we build the net weight update corresponding to the removal of multiple parameters by adding the optimal weight update, Eqn. (2.11), computed separately for each parameter that we decide to prune. However, note that we will have to apply a mask on this weight update so as to adjust for adding the weight updates considered separately. Otherwise, the weight for the pruned parameters after applying the update might not be zero. We will call this resulting weight update as the pruning direction.

2.2.3 Cases for specific kinds of Hessian

Optimal Brain Damage (LeCun et al., 1990). If the hessian is assumed to be diagonal, then we can write the above Eq. (2.12) as follows:

$$\delta L_{\text{OBD}}^* = \frac{1}{2} w_q^2 [\mathbf{H}]_{qq}. \quad (2.20)$$

Magnitude Pruning. On top of the above case, if we assume the hessian is identity³, then we can write the above Eq. (2.12) as follows:

$$\delta L_{\text{Mag}}^* = \frac{1}{2} w_q^2. \quad (2.21)$$

2.3 Related Work

While in this chapter, we have mainly focussed on the Optimal Brain Damage/Surgeon framework from [LeCun et al. \(1990\)](#); [Hassibi and Stork \(1993\)](#) which performs pruning in a single-shot, there are many other approaches to achieving model compression. We highlight some of these in our discussion ahead. For an extensive survey, we refer the readers to [Cheng et al. \(2017\)](#).

Gradual pruning. Methods of this kind interleave rounds of re-training between smaller pruning steps and gradually or incrementally achieve the set target of sparsity. Many works adopting this technique ([Han et al., 2015](#); [Zhu and Gupta, 2017](#); [Gale et al., 2019](#)) have achieved impressive results, and has now become one of the standard approaches for pruning. Most of these methods use magnitude pruning as the principal tool for pruning, which has essentially led to the community ignoring Hessian-based approaches. Other variants of this approach have tried to correct for non-optimally removed parameters via magnitude-pruning by using some re-introduction heuristics as in [Guo et al. \(2016\)](#); [Mostafa and Wang \(2019\)](#). Overall, an important factor for the adoption of magnitude pruning has been the lack of efficient Hessian based alternatives, which we seek to address via our work (c.f. Section 4.3).

Sparsity regularization during training. These methods ([Louizos et al., 2017](#); [Carreira-Perpinán and Idelbayev, 2018](#)) impose a sparsity penalty during the training of neural networks, like ℓ_0 or ℓ_1 regularization which are known to encourage sparsity. Post-training parameters with smaller magnitudes are removed. Other works have looked at this from the Bayesian perspective ([Molchanov et al., 2017](#)), where the dropout probabilities are learned for each weights, which are eventually used to decide which parameters to remove. However, methods of this kind suffer due to the manual tuning required for the regularization hyper-parameters, the optimal value of which might differ from layer to layer. Further, these methods can

³Or a constant multiple of identity, it remains equivalent to magnitude pruning

sometimes require more iterations to converge and might not still attain the performance level of unstructured pruning (Cheng et al., 2017; Gale et al., 2019).

Structured pruning. These methods (Luo et al., 2017; Li et al., 2016; Theis et al., 2018) have been motivated to yield an out-of-the-box speed-up in the inference time by removing parameters in a structured manner, such as removing entire channels or neurons. This is in contrast to the unstructured pruning methods that we talked above which require sparse convolutional kernels to result in a speed-up at inference. Nevertheless, it has been observed that the best results, as well as higher levels of pruning, are obtained via unstructured pruning methods, which is our focus throughout this work.

Dynamic pruning. Dynamic pruning methods (Mostafa and Wang, 2019; Dettmers and Zettlemoyer, 2019; Lin et al., 2020) strive to maintain a sparse model throughout training in comparison to first training a dense model and then pruning it. Typically these methods carry out a cycle of prune-redistribute-regrowth along with usual training, either continuously or at regular intervals. Similar to gradual pruning methods, the principal tool used for removing parameters is magnitude-based pruning. This kind of sparse-to-sparse pruning paradigm reduces the involved training costs, but deep learning frameworks like PyTorch or TensorFlow represent these models as dense, leading to minimal performance gains. Further, it should be kept in mind that pruning a dense model needs to be performed only once, and thus the additional cost incurred in gradual pruning is amortized, and will not be an issue if it can provide an improvement in accuracy over dynamic pruning methods. Lastly, the development of a better one-shot pruning method than magnitude pruning will prove beneficial to methods of this type as well.

Model fusion based methods. In this line of work, one or more big models (teacher networks) are fused together to result in a single compact model (student network). This can be achieved by matching the softmax outputs of the teacher and student networks as in distillation (Hinton et al. (2015)), or aligning and fusing intermediate or output layers via optimal transport (Singh and Jaggi, 2019) or by weight sharing (Chou et al., 2018) and fine-tuning. The principal method in this category, distillation, suffers from high computational costs and as a result of which other methods of this kind have remained relatively unused as compared to gradual and dynamic pruning methods. Nevertheless, these methods do possess the potential to become a frequent occurrence in model compression.

Compressing the representation of weights. Methods of this category reduce the memory footprint of the parameter weights by quantizing their values (Han et al. (2015)) instead of employing the usual 32-bit floating-point representation. In a different approach, HashedNets (Chen et al., 2015) compresses the parameter representation by grouping connection weights into hash buckets, all of which share a single parameter value. These methods are however

Chapter 2. Model Compression

independent of the other compression methods discussed above, and can be further used alongside.

3 Efficient IHVP approximation

In the previous chapter, we discussed the relationship between Hessian, Fisher, and Gauss-Newton matrices and how they are equivalent when the model and data distribution match. We can also use these other related matrices in place of the Hessian to define the local quadratic model (Eqn. (1.5)).

A practical advantage of Fisher is that it is positive semi-definite (PSD), while there is no such guarantee for the Hessian. This implies that Fisher is guaranteed to be invertible assuming we simply add a small multiple of the identity matrix to make it positive definite. The same applies to the empirical Fisher. For the Gauss-Newton matrix, this holds as long as the hessian \mathbf{H}_ℓ of the loss ℓ with respect to the network output f is positive semi-definite, which is true in the case of convex loss functions (like mean-squared error).

While the empirical Fisher does not share the equivalence with the Gauss-Newton like the true Fisher, it can, however, be built much more efficiently. Further, during the course of training, the gradient of the objectives are anyways calculated. In comparison, the true Fisher would require m additional back-propagation steps for each sampled \mathbf{y} or k more steps to compute the Jacobian¹.

Thus, as a first check, let's see how the Hessian and empirical Fisher matrices behave in practice. Are they close enough to even merit discussion? If so, how can we efficiently estimate the inverse Hessian-vector products (IHVPs) via the use of empirical Fisher?

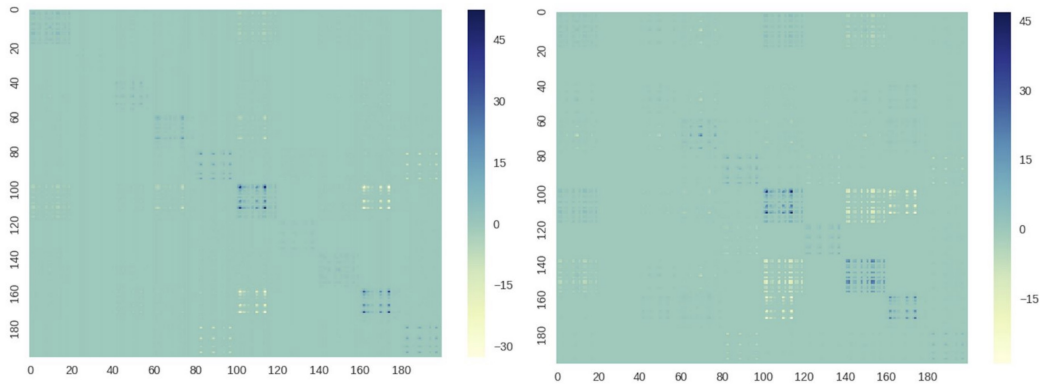
3.1 A visual exploration of Hessian and empirical Fisher matrices

3.1.1 On MNIST

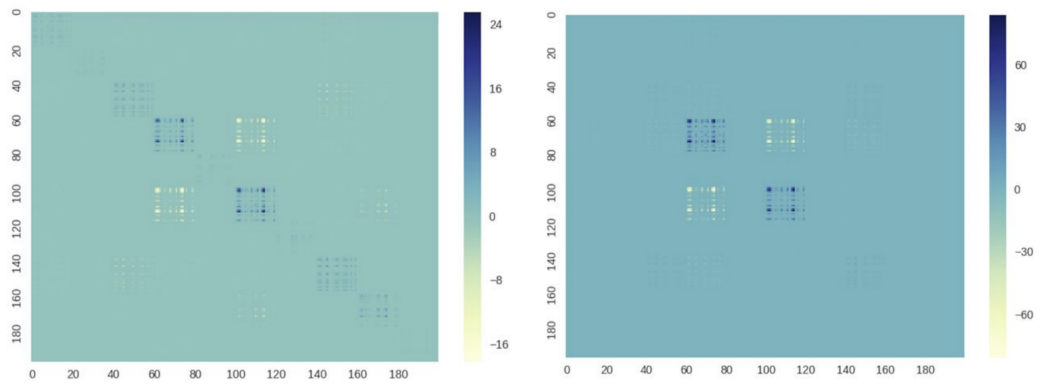
For our experimental setup, we first consider a fully-connected network trained on the MNIST digit recognition dataset. This fully-connected network has two hidden layers of size 40 and

¹This is the case when a closed-form for \mathbf{H}_ℓ can be computed, like for exponential distributions. Refer to the Section 1.6 for more details.

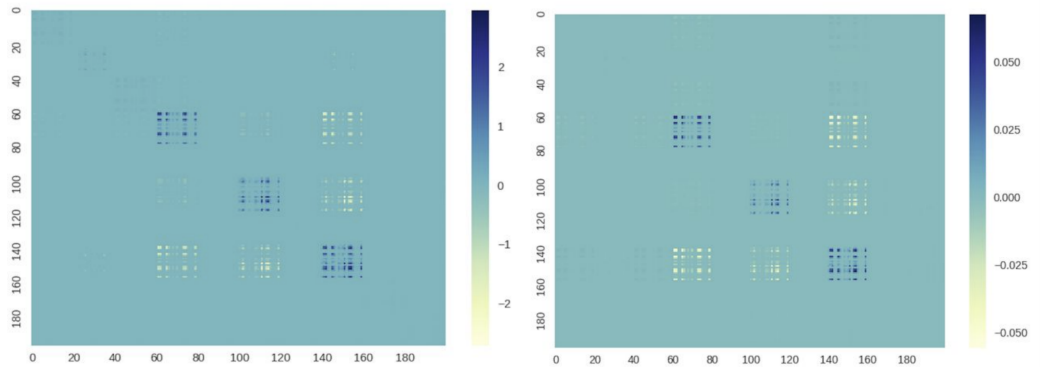
Chapter 3. Efficient IHVP approximation



(a) At 0.5 epochs. Test accuracy at this stage is 63.9%.



(b) At 5 epochs. Test accuracy at this stage is 85.5%.



(c) At 50 epochs. Test accuracy at this stage is 90.6%.

Figure 3.1 – Last-layer Hessian and empirical Fisher blocks for MLPNET ($784 \rightarrow 40 \rightarrow 20 \rightarrow 10$) at different points of training on MNIST. Both Hessian and empirical Fisher have been estimated over a batch of 64 examples in all the figures. Hessian blocks are in the left-column, while empirical Fisher blocks are displayed in the right-column.

20. MNIST consists of 28×28 grayscale images for the digits 0 – 9. Thus the overall shape of this network can be summarized as $784 \rightarrow 40 \rightarrow 20 \rightarrow 10$.

3.1. A visual exploration of Hessian and empirical Fisher matrices

Note, here our purpose is not to get the best test accuracy, but rather we would like to inspect the structures of the Hessian and the empirical Fisher matrices. As a result, we choose the network with a relatively small size so as to exactly compute the full Hessian via double back-propagation. We use stochastic gradient descent (SGD) with a constant learning rate of 0.001 and a momentum of 0.5 to train this network. The training set was subsampled to contain 5000 examples in order to prototype faster, and the batch size used during optimization was 64.

In Figure 3.1, we compare the last-layer sub-matrices of sizes 200×200 for both Hessian and empirical Fisher at different stages of training. We see that both these matrices share a significant amount of similarities in their structure. In other words, if we were to compute say the correlation or cosine similarity between the two matrices, it would be quite high. In these plots, the number of samples used to build the estimates of Hessian and empirical Fisher was 16, and similar trends can be observed if more samples are taken.

One might argue that these results are for MNIST and the trend might not hold when we move to a more realistic dataset like CIFAR10. Also, currently, we have only inspected the plots for last-layer sub-matrix and possibly things could be different when we look at other diagonal and off-diagonal/cross blocks.

So let's move to CIFAR10 and see how these results actually hold there as well. Likewise, a similar structure of the Hessian and empirical Fisher can be seen for other diagonal and off-diagonal blocks.

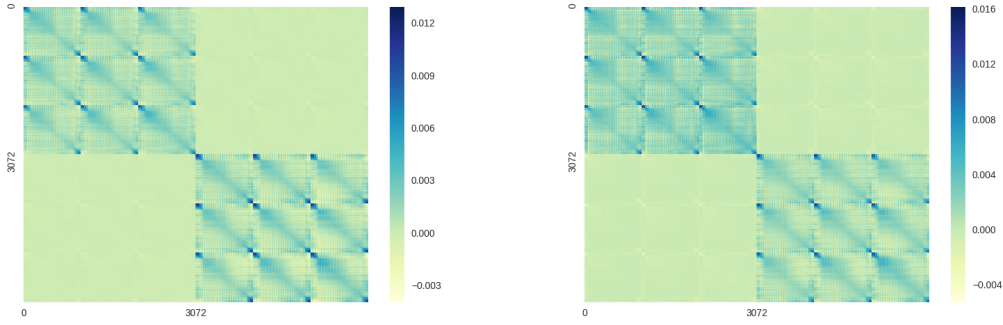
3.1.2 On CIFAR10

Again we consider a fully connected network with two hidden layers. CIFAR10 consists of 32×32 RGB images and so we adapt the size of network to as follows: $3072 \rightarrow 16 \rightarrow 64 \rightarrow 10$. We refer to this network as CIFARNET. As explained before, such a size is chosen for computational reasons, as the full Hessian exactly is very expensive to compute.

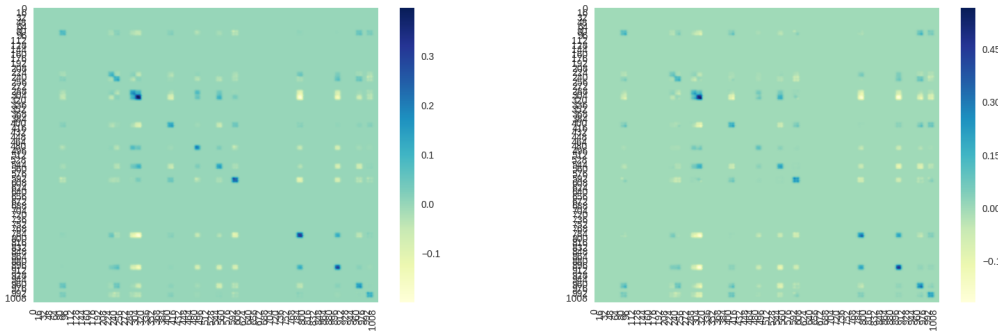
We follow a commonly used SGD-based optimization schedule for training this network on CIFAR10, with a learning rate 0.05 which is decayed by a factor of 2 after every 30 epochs, momentum 0.9, and train it for a total of 300 epochs. The checkpoint with best test accuracy is used as a final model, and this test accuracy² is 41.8%. However, this low test accuracy is not a concern for us, as we are more interested in investigating the structures of the Hessian and the empirical Fisher matrices.

The plots in the Figure 3.2 illustrate the obtained matrices for the diagonal sub-matrices corresponding to the first, second, and the third layers. We observe that empirical Fisher possesses essentially the same structure as observed in the Hessian. Further, Figure 3.3 presents the result for the off-diagonal or cross blocks of these two matrices, where also we

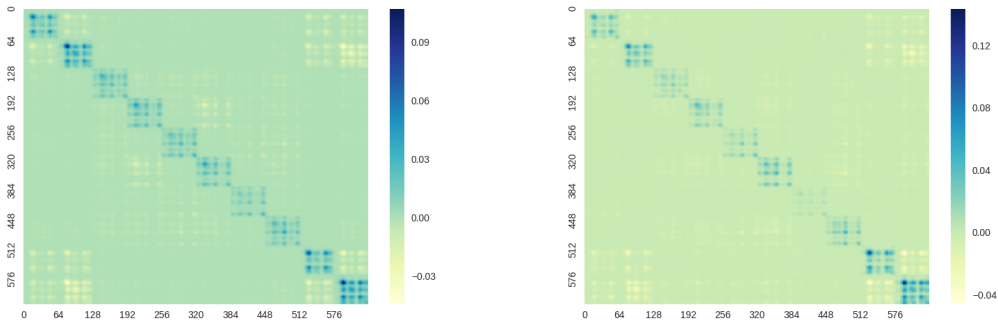
²In fact, this CIFARNET model with 41.8% test accuracy, is far from ensuring that the model and data distribution match, yet the empirical Fisher is able to faithfully capture the structure of the Hessian.



(a) First-layer sub matrices averaged across over diagonal blocks of 6144×6144 for illustration purposes.



(b) Second-layer sub-matrices.

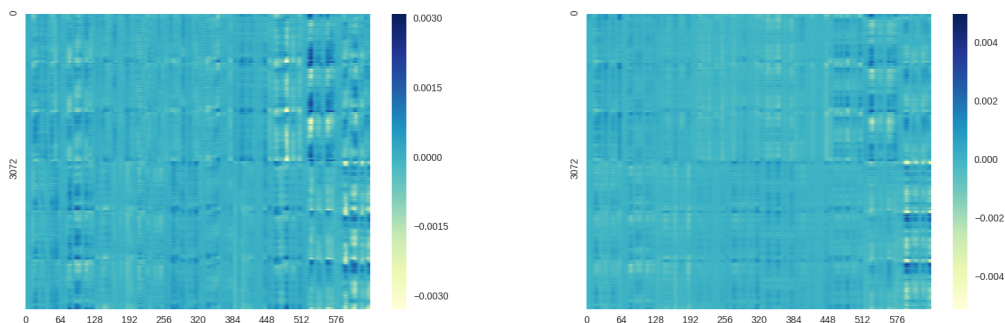


(c) Third-layer sub matrices.

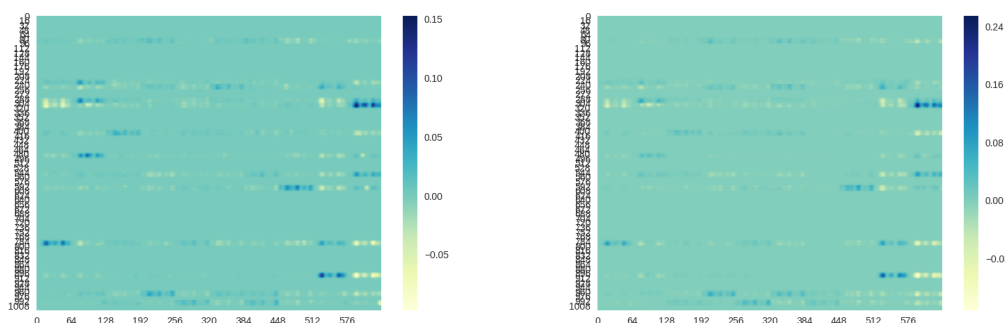
Figure 3.2 – **Diagonal** Hessian and empirical Fisher blocks for CIFARNET ($3072 \rightarrow 16 \rightarrow 64 \rightarrow 10$) corresponding to different layers when trained on CIFAR10. Figures have been smoothed slightly with a Gaussian kernel for better visibility. Both Hessian and empirical Fisher have been estimated over a batch of 100 examples in all the figures. Hessian blocks are in the left-column, while empirical Fisher blocks are displayed in the right-column.

find a similar trend.

Thus, we conclude that the empirical Fisher shares the structure present in the Hessian matrix.



(a) First-layer and third-layer cross matrices averaged across over blocks of 6144×640 for illustration purposes.



(b) Second-layer and third-layer cross matrices.

Figure 3.3 – **Off-Diagonal** Hessian and empirical Fisher blocks for CIFARNET ($3072 \rightarrow 16 \rightarrow 64 \rightarrow 10$) corresponding to different layers when trained on CIFAR10. Figures have been smoothed slightly with a Gaussian kernel for better visibility. Both Hessian and empirical Fisher have been estimated over a batch of 100 examples in all the figures. Hessian blocks are in the left-column, while empirical Fisher blocks are displayed in the right-column.

In the coming section, we focus on the other question which we posed at the beginning of this chapter. Namely, how can we efficiently estimate the inverse?

3.2 Inverting the empirical Fisher

As discussed before, we can simply add a small scalar factor of the identity to guarantee the invertibility of the empirical Fisher. Then, a naive way to compute its inverse would be to first build the empirical Fisher matrix itself and then use standard inversion techniques, like Gaussian elimination.

The foremost thing to note is that in most use-cases where we consider a local quadratic model via some curvature matrix, we only need its inverse. This is typically in the form of inverse matrix-vector products. Thus, we would like to have a method that does not require the full

Chapter 3. Efficient IHVP approximation

matrix in the first place to compute the inverse.

The second point is that usual techniques do not work for us, as their runtime complexity is cubic in the dimension, which is out of the question for the case of neural networks which have dimensionality in the orders of millions.

Woodbury Matrix Identity: We consider the Woodbury matrix identity which gives the formula for computing the inverse of a particular correction to a given invertible matrix A . Let us suppose that we are given two invertible matrices A and C of sizes $d \times d$ and $k \times k$ respectively. Further, we have two additional matrices: U of size $d \times k$ and V of size $k \times d$. Then, the inverse of $A + UCV$ can be computed as follows,

$$(A + UCV)^{-1} = A^{-1} - A^{-1}U(C^{-1} + VA^{-1}U)^{-1}VA^{-1}. \quad (3.1)$$

Further, if we assume C to be the identity matrix and consider U and V as vectors, we can rewrite the above to,

$$(A + \mathbf{u}\mathbf{v}^\top)^{-1} = A^{-1} - \frac{A^{-1}\mathbf{u}\mathbf{v}^\top A^{-1}}{1 + \mathbf{v}^\top A^{-1}\mathbf{u}}. \quad (3.2)$$

This particular variant also goes by the name of Sherman-Morrison formula. Recalling, the form of the empirical Fisher matrix, we can express it as the following recurrence:

$$\hat{F}_{n+1} = \hat{F}_n + \frac{1}{N} \nabla \ell_{n+1} \nabla \ell_{n+1}^\top, \quad \text{where } \hat{F}_0 = \lambda I_d. \quad (3.3)$$

In the above equation, λ denotes the dampening term we consider, i.e., we add a positive scalar λ times the identity matrix I_d to make the the empirical Fisher positive definite. Then comparing with the Eqn. (3.2) above, we can write a recurrence for calculating the inverse of empirical Fisher as follows,

$$\hat{F}_{n+1}^{-1} = \hat{F}_n^{-1} - \frac{\hat{F}_n^{-1} \nabla \ell_{n+1} \nabla \ell_{n+1}^\top \hat{F}_n^{-1}}{N + \nabla \ell_{n+1}^\top \hat{F}_n^{-1} \nabla \ell_{n+1}}, \quad \text{where } \hat{F}_0^{-1} = \lambda^{-1} I_d. \quad (3.4)$$

Finally, we can express the inverse of the empirical Fisher as shown below,

$$\hat{F}^{-1} = \left(\lambda I_d + \frac{1}{N} \sum_{n=1}^N \nabla \ell_n \nabla \ell_n^\top \right)^{-1} = \hat{F}_{N+1}^{-1}. \quad (3.5)$$

The advantage of using such an approach is that it is quadratic in dimensionality in comparison to cubic for standard inversion methods. Also, we note that while the above formula goes

3.3. Approximation quality of the local quadratic model

until $n = N$, in practice, we only need a small subset of examples, m , which typically ranges between 100 to 1000. Thus, the runtime of this Woodbury-based inverse is $\mathcal{O}(md^2)$.

Yet, this would still be large when neural networks are concerned which have parameters in the range of hundreds of millions. We thus need to employ a block-wise assumption on the Fisher, where we instead consider smaller blocks on the diagonal and ignore the off-diagonal parts. Given the huge size of neural-networks, making the block-wise assumption is now an accepted practice. Then, if we assume that we have uniform blocks of size $c \times c$ along the diagonal, then the runtime of this inversion operation would become $\mathcal{O}(mcd)$, and hence linear in dimensionality d (which would be the bare minimum).

Remark: We also note that a Woodbury-based inverse can also be used for the true Fisher. This holds if the Hessian \mathbf{H}_ℓ of the loss ℓ with respect to the function output f is positive semi-definite (or the loss ℓ is convex in f). Then via equivalence to Gauss-Newton (Eqn. (1.16)), the true Fisher matrix is given by,

$$F = \frac{1}{N} \sum_n J_n \mathbf{H}_\ell J_n^\top, \quad (3.6)$$

where, J_n denotes the Jacobian $J_n = J_{\mathbf{w}} f(\mathbf{x}_n; \mathbf{w})$. Thus, we can develop a recurrence for it similar to Eqn. (3.3). Then instead of employing the Sherman-Morrison variant, we will have to use the full-fledged Woodbury matrix identity (Eqn. (3.1)). But, this will of course come at the cost of increasing the runtime by the number of function outputs, k (e.g., for ImageNet k would be 1000).

3.3 Approximation quality of the local quadratic model

In order to evaluate the accuracy of our local quadratic model, when used along with empirical Fisher and inverse estimated via the Woodbury identity (as in Eqn. (3.4)), we compare how does the loss predicted by it compares against the actual training loss. We will refer to this method of building a local quadratic model with empirical Fisher in place of Hessian and its inverse compute via Woodbury as **WoodFisher** hereafter.

We test it on three different directions, where each corresponds to the pruning direction (weight update) obtained when compressing a particular layer to 50% sparsity. We choose three layers from different stages of network for ResNet-20 on CIFAR-10, i.e., {'layer1.0.conv1', 'layer2.0.conv1', layer3.0.conv1'}.

Figure 3.4 presents the results for these experiments. We observe that for all the three cases, the local quadratic model using WoodFisher predicts an accurate approximation to the actual underlying loss. The corresponding dampening used can be adjusted depending on whether a more conservative or relaxed estimate of the training loss is needed. This assures us about the effectiveness of our approach and we demonstrate its application extensively for model compression in the next chapter.

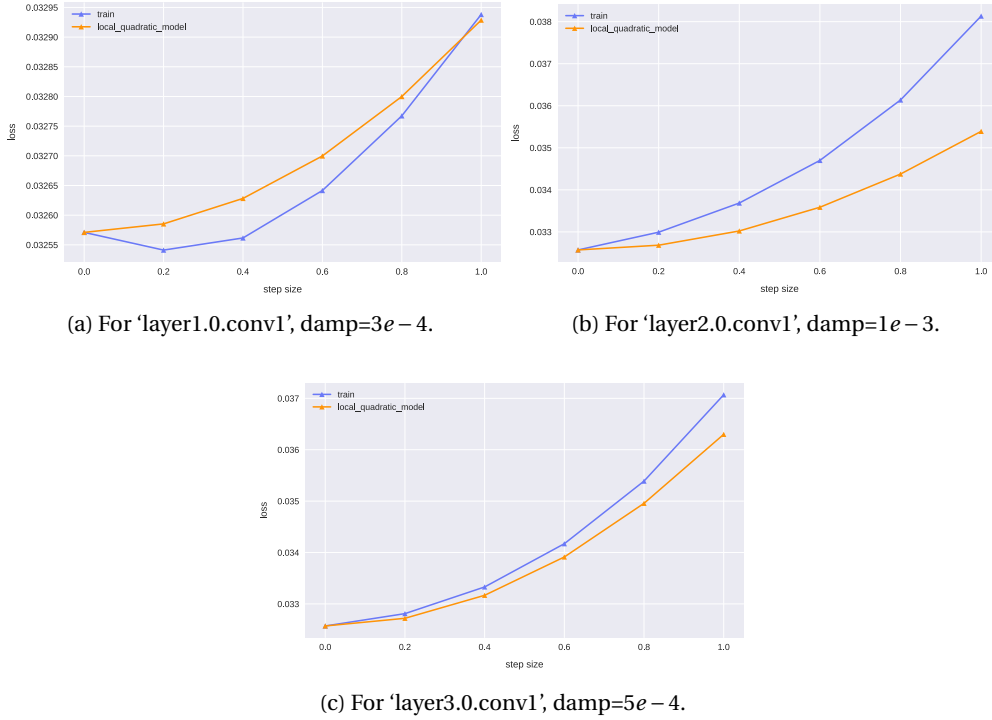


Figure 3.4 – Approximation quality of the loss suggested by the local quadratic model using WoodFisher with respect to the actual training loss. The three plots represent three different directions along which the quality of local quadratic model is measured, which correspond to the pruning direction obtained by pruning the layers: {'layer1.0.conv1', 'layer2.0.conv1', 'layer3.0.conv1'} to 50% sparsity.

3.4 Discussion

3.4.1 Suitability of the Empirical Fisher

Recently, [Kunstner et al. \(2019\)](#) have raised arguments about the limitations of the empirical Fisher information, which might seem conflicting with the proposal here. Thus, we do a breakdown of their arguments and discuss how some of them are not really valid.

Going back to the least-squares example in Section 1.6, the expressions for the empirical and true Fisher in this setting are shown below in Eqns. (3.7) and (3.8) respectively.

$$\hat{\mathbf{F}} = \frac{1}{N} \sum_n r_n^2 \nabla f(\mathbf{x}_n; \mathbf{w}) \nabla f(\mathbf{x}_n; \mathbf{w})^\top \quad (3.7)$$

$$\mathbf{F} = \frac{1}{N} \sum_n \nabla f(\mathbf{x}_n; \mathbf{w}) \nabla f(\mathbf{x}_n; \mathbf{w})^\top \quad (3.8)$$

Eqn. (3.8) follows via the equivalence of true Fisher to the Gauss-Newton (see (1.16)) and the fact the $\mathbf{H}_\ell = I$ for least-squares.

(1) *Consequently, the authors argue that as residuals approach zero, the empirical Fisher goes to zero. But the (true) Fisher approaches the Hessian.*

However, this conclusion rests on the assumption that each individual gradient vanishes, which is not true. Only the average gradient goes to zero.

The other term in the Gauss-Newton does go to zero, if the $\nabla_f \ell_n = r_n$ and $\nabla^2 f(\mathbf{x}_n; \mathbf{w})$ are assumed to be uncorrelated (Sagun et al., 2018). So essentially, the empirical Fisher differs from the Hessian only by the scaling of outer-products in this setting, but the underlying structure is maintained.

(2) *The other argument that the authors make is that model needs to be realizable,³ as well as a large number of samples, are needed to ensure the consistency of the maximum likelihood estimate.*

However, as reflected in our empirical results i.e., similarities of the Hessian and empirical Fisher structures on MNIST and CIFAR10, the accuracy of the local quadratic model for ResNet-20 on CIFAR10, as well as other model compression results presented later in Chapter 4, these conditions are satisfied in the practical scenario.

Note that, in contrast to the empirical Fisher, we need a lot more back-propagation steps to compute the true Fisher. This might be either in the form of m more steps needed for each sampled \mathbf{y} . Or the number of output, k , many additional steps to compute the Jacobian, assuming the Hessian \mathbf{H}_ℓ can be computed in closed form.

Conclusion: As a result, we conclude that empirical Fisher is a lot more efficient than true Fisher, while still giving a faithful estimate of the Hessian structure.

3.4.2 Issues with using K-FAC

In the recent years, another kind of approximation called K-FAC (Heskes, 2000; Martens and Grosse, 2015) has been made for the Fisher that results in a more efficient application when used as a pre-conditioner or for IHVPs. Consider we have a fully-connected network with l layers. If we denote the pre-activations of a layer i by \mathbf{s}_i , we can write them as $\mathbf{s}_i = W_i \mathbf{a}_{i-1}$, where W_i is the weight matrix at the i^{th} layer and \mathbf{a}_{i-1} denotes the activations from the previous layer (which the i^{th} layer receives as input).

By chain rule, the gradient of the objective L with respect to the weights in layer i , is the following: $\nabla_{W_i} L = \text{vec}(\mathbf{g}_i \mathbf{a}_{i-1}^\top)$. Here, \mathbf{g}_i is the gradient of the objective with respect to the pre-activations s_i of this layer, so $\mathbf{g}_i = \nabla_{s_i} L$. Using the fact that $\text{vec}(\mathbf{u}\mathbf{v}^\top) = \mathbf{v} \otimes \mathbf{u}$, where \otimes

³Realizability means that a setting of parameters exists such that the model and data distribution match.

Chapter 3. Efficient IHVP approximation

denotes the Kronecker product, we can simplify our expression of the gradient with respect to W_i as $\nabla_{W_i} L = \mathbf{a}_{i-1}^\top \otimes \mathbf{g}_i$.

Then, we can then write the Fisher block corresponding to layer i and j as follows,

$$F_{i,j} = \mathbb{E}[\nabla_{W_i} L \nabla_{W_j} L^\top] = \mathbb{E}\left[(\mathbf{a}_{i-1} \otimes \mathbf{g}_i)(\mathbf{a}_{j-1} \otimes \mathbf{g}_j)^\top\right] \stackrel{(a)}{=} \mathbb{E}\left[(\mathbf{a}_{i-1} \otimes \mathbf{g}_i)(\mathbf{a}_{j-1}^\top \otimes \mathbf{g}_j^\top)\right] \stackrel{(b)}{=} \mathbb{E}\left[\mathbf{a}_{i-1} \mathbf{a}_{j-1}^\top \otimes \mathbf{g}_i \mathbf{g}_j^\top\right], \quad (3.9)$$

where, in (a) and (b) we have used the transpose and mixed-product properties of Kronecker product. The expectation is taken over the model's distribution as in the formulation of Fisher.

The Kronecker Factorization (K-FAC) based approximation \tilde{F} thus used by the authors can be written as,

$$\tilde{F}_{i,j} = \mathbb{E}\left[\mathbf{a}_{i-1} \mathbf{a}_{j-1}^\top\right] \otimes \mathbb{E}\left[\mathbf{g}_i \mathbf{g}_j^\top\right] = \tilde{A}_{i-1,j-1} \otimes \tilde{G}_{i,j} \quad (3.10)$$

Essentially, we have moved the expectation inside and do it prior to performing the Kronecker product. As mentioned by the authors, this is a major approximation since in general the expectation of a Kronecker product is not equal to the Kronecker product of the expectations. We will refer to \tilde{F} as the Fisher matrix underlying K-FAC or the K-FAC approximated Fisher.

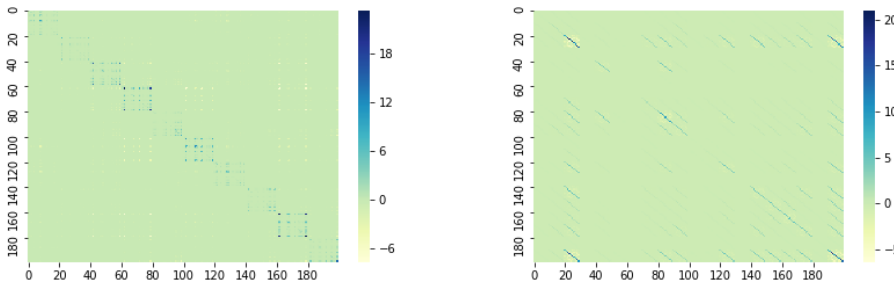


Figure 3.5 – **Left:** Last-layer sub-matrix of the empirical Fisher. **Right:** Last-layer sub-matrix for the K-FAC approximated Fisher. We see that the K-FAC approximated Fisher loses a lot of the structure present in the empirical Fisher (as well as the Hessian from our analysis in Section 3.1).

The advantage of such an approximation is that it allows to compute the inverse of K-FAC approximated Fisher quite efficiently. This is because the inverse of a Kronecker product is equal to the Kronecker product of the inverses. This implies that instead of inverting one matrix of bigger size $n_{i-1}n_i \times n_{j-1}n_j$, we need to invert two smaller matrices $\tilde{A}_{i,j}$ and $\tilde{G}_{i,j}$ of sizes $n_{i-1} \times n_{j-1}$ and $n_i \times n_j$ respectively (here, we have denoted the number of neurons in layer ℓ by n_ℓ).

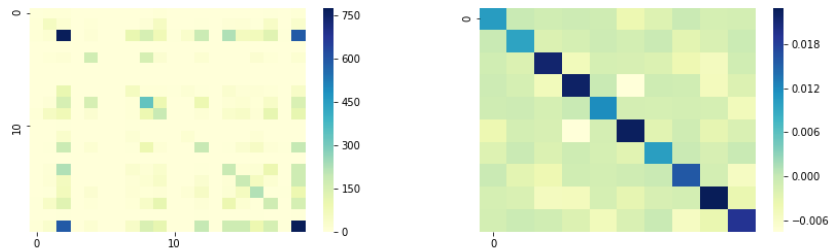


Figure 3.6 – The Kronecker factors $\tilde{A}_{3,3}$ and $\tilde{G}_{3,3}$ of sizes 20×20 and 10×10 are displayed in the left and right columns respectively. These two matrices undergo a Kronecker product to yield the K-FAC approximated Fisher as in the right plot of Figure 3.5.

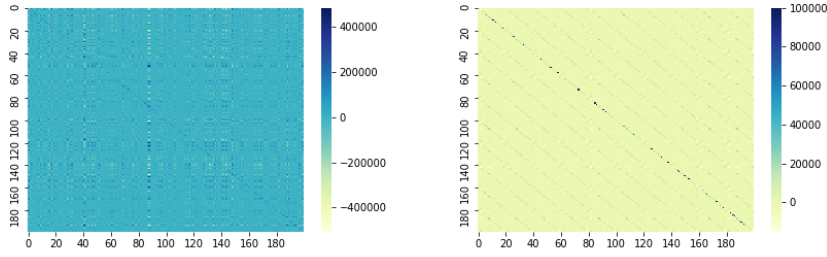
As a result, K-FAC has found several applications in the last few years in: optimization (Ba et al., 2016; Osawa et al., 2019), pruning (Zeng and Urtasun, 2019; Wang et al., 2019), reinforcement-learning (Wu et al., 2017), etc. However, an aspect that has been ignored is the accuracy of this approximation as compared to using the real Fisher. We discuss this aspect in detail ahead as well as a few more challenges associated with the Kronecker-factorization based approaches.

Quality of the approximation. We perform a qualitative analysis to evaluate the accuracy of this approximation. As in Section 3.1, we consider the MLPNET on MNIST and build the full (empirical) Fisher and K-FAC approximated Fisher matrices. Figure 3.5 illustrates the difference between the two matrices for the last-layer sub-matrix. We observe that the K-FAC approximated Fisher grossly deviates from true structure underlying the empirical Fisher, and thus from the Hessian too as concluded in our analysis of Section 3.1.

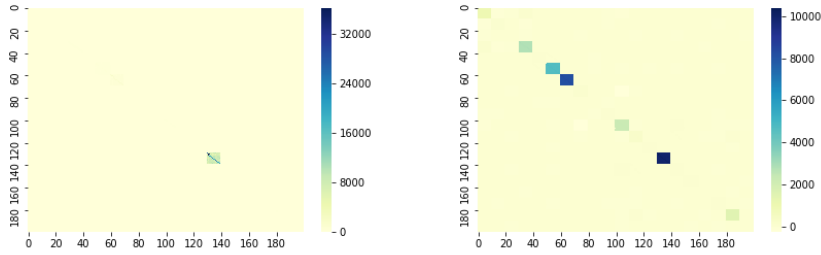
Note that this structure for the K-FAC approximated Fisher is kind of expected since it is the Kronecker product of the two smaller matrices $\tilde{A}_{i,j}$ and $\tilde{G}_{i,j}$, which are also presented in Figure 3.6 for the setting of Figure 3.5 (where we consider $i = j = 3$, i.e., the third layer). We would like to remark that the results are similar even if we instead use a y sampled from the model’s distribution as suggested in the K-FAC paper.

It might be argued that since we are anyways interested in the inverse of the Fisher, maybe this difference in approximation does not matter there. We show in Figure 3.7 that this is not true. In fact, there is a significant difference when compared with the inverse of this third-layer sub-matrix, either performed together with the full matrix or separately as a block. Figure 3.7 included the results of K-FAC based inverse for two variants of dampening proposed in the original paper.

Extending to different network types. Another issue with K-FAC is that it only naturally exists for fully-connected networks. When one proceeds to the case of convolutional or recurrent neural networks, the Kronecker structure needs to be specially designed by making further



(a) **Left:** $(\hat{F}^{-1})_{3,3}$ i.e., when empirical Fisher is inverted as whole. **Right:** $(\hat{F}_{3,3})^{-1}$ i.e., when just the corresponding block of empirical Fisher is inverted.



(b) **Left:** Inverse of K-FAC approximated Fisher with dampening hyper-parameter $\pi = 1$. **Right:** Inverse of K-FAC approximated Fisher with dampening hyper-parameter π is calculated from its mentioned formula.

Figure 3.7 – Comparison of the inverse of last-layer sub-matrix obtained via empirical Fisher (**Top**) and K-FAC (**Bottom**). In all the figures, dampening used is $1e-5$.

approximations (Grosse and Martens, 2016; Martens et al., 2018). Whereas, a WoodFisher based method would not suffer from such a problem.

Application to larger networks. Furthermore, when applied to the case of large neural networks like ResNet-50, often further approximations like the chunking of block size as we consider or channel-grouping as called by Laurent et al. (2018), or assuming spatially uncorrelated activations are anyways required.

Thus, in lieu of these aspects, we argue that WoodFisher, i.e., (empirical) Fisher used along with Woodbury-based inverse, is a better alternative since it maintains the efficiency while being faithful to the underlying structure of the Hessian.

3.5 Other approximation methods

There is a huge body of work aimed at utilizing second-order information in machine learning and optimization. To the extent that it would be infeasible to discuss each and every available method. In the section, we discuss some of the most relevant lines of work that can be used for estimating inverse Hessian-vector products (IHVPs).

Double back-propagation. This forms the naive way of computing the entire Hessian matrix by explicitly computing each of its entries. However, such an approach is extremely slow and would require $\mathcal{O}(d^2)$ back-propagation steps, each of which has a runtime of $\mathcal{O}(md)$, where m is the size of the mini-batch considered. Thus, this cubic time approach is out of the question.

Diagonal Hessian. If we assume the Hessian to be diagonal, this allows us to compute the inverse very easily by simply inverting the elements of the diagonal. But, even if we use the Pearlmutter’s trick (Pearlmutter, 1994), which lets us compute the exact Hessian-vector product in linear time, we need a total of $\mathcal{O}(d)$ such matrix-vector products to estimate the diagonal, which results in an overall quadratic time.

Diagonal Fisher. Diagonal estimate for the empirical Fisher is really efficient to build, since it just requires computing the average of the squared gradient across the training samples, for each dimension. If the mini-batch size is m , we just need $\mathcal{O}(md)$ time to build this estimate. This approach has been widely used in optimization by adaptive methods (Kingma and Ba, 2014; Duchi et al., 2010), as well for model compression by the work called Fisher-pruning (Theis et al., 2018). However as we show ahead, by simply paying a small additional factor of c in the runtime, we can estimate the inverse and IHVPs more accurately. This leads to a performance which is significantly better than that obtained via diagonal Fisher.

Hessian-Free methods. Another line of work is to completely forgo the explicit computation of Hessians (Martens, 2010), by posing the problem of computing IHVP with a vector \mathbf{v} as solving the linear system $\mathbf{H}\mathbf{x} = \mathbf{v}$ for \mathbf{x} . Such methods rely on conjugate-gradients based linear-system solvers that only require matrix-vector products, which for neural networks can be obtained via Pearlmutter’s trick (Pearlmutter, 1994). However, a big disadvantage of these methods is that they can require a lot of iterations to converge since the underlying Hessian matrix is typically very ill-conditioned. Further, this whole procedure would have to be repeated at least $\mathcal{O}(d)$ times to build just the diagonal of the inverse, which is the minimum needed for application in model compression.

Neumann series expansion. These kind of methods (Krishnan et al., 2018; Agarwal et al., 2016) essentially exploit the following result in Eqn. (3.11) for matrices A which have an eigen-spectrum bounded between 0 and 1, i.e., $0 < \lambda(A) < 1$.

$$A^{-1} = \sum_{i=0}^{\infty} (I - A)^i \tag{3.11}$$

This can be then utilized to build a recurrence of the following form,

$$A_n^{-1} \triangleq I + (I - A)A_{n-1}^{-1}, \tag{3.12}$$

Chapter 3. Efficient IHVP approximation

which allows us to efficiently estimate (unbiased) IHVP's via sampling. However, an important issue here is the requirement of the eigen-spectrum to be between 0 and 1, which is not true by default for the Hessian. This implies that we further need to estimate the largest absolute eigenvalue (to scale) and the smallest negative eigenvalue (to shift). Hence, requiring the use of the Power method which adds to the cost. Further, the Power method might not be able to return the smallest negative eigenvalue at all, since when applied to the Hessian (or its inverse) it would yield the eigenvalue with the largest magnitude (or smallest magnitude).

K-FAC. Kronecker-factorization based approximation ([Heskes, 2000](#); [Martens and Grosse, 2015](#)) to the Fisher have gained traction in recent times, but as highlighted in the previous Section 3.4.2, the main issue is that it misrepresents the underlying structure of the Hessian.

Woodbury-based methods. In prior work, Woodbury-based inverse has been considered for the case of a one-hidden layer neural network in Optimal Brain Surgeon (OBS, [Hassibi and Stork \(1993\)](#)), where the analytical expression of the Hessian can be written as an outer product of gradients. An extension of this approach to deeper networks was proposed in [Dong et al. \(2017\)](#), by defining separate layer-wise objectives, where the expression of the layer Hessian becomes similar to that in OBS. We follow a similar inspiration but exploit the relation of the empirical Fisher matrix with the Hessian, to generalize this approach in the case of deep neural networks.

4 Experiments

In this section, we apply our method, WoodFisher, to compress multi-layer perceptrons (MLPs), convolutional neural networks (CNNs), and residual networks, on standard image classification datasets like MNIST, CIFAR10, ImageNet. We consider two modes for the application of WoodFisher:

(a) Independent mode: In this approach, we make the choice of selecting the parameters to prune independently or separately in each layer. This requires that we specify the pruning levels for each layer. A common way is to prune all the layers uniformly, i.e., at the same level. Sometimes, different methods exclude certain layers (like the input or the output) which are known to be sensitive, or carry-out a proper sensitivity analysis to decide these pruning levels for each layer.

(b) Joint (or Global) mode: Here, the decision to prune which parameters is made jointly across all the layers. This means that we compute the pruning-statistic via Eqn. (2.13) for all the parameters in the network and then remove those parameters which have the lowest values of this statistic.

The advantage of this approach is that the pruning levels for each layer are thus decided automatically based on the comparison of pruning-statistic across the layers. So, we can simply specify a global target of how much sparsity we want, and the pruning-statistic in this joint mode takes care of the rest.

Organization. We first discuss the results for the setting of one-shot pruning in Section 4.1. Then we present some ablation studies in Section 4.2 to understand the effect of block-wise assumptions on the performance of WoodFisher. Lastly, in Section 4.3 we also apply WoodFisher in the setting of gradual pruning and see where it ranks in comparison to recent start-of-the-art methods.

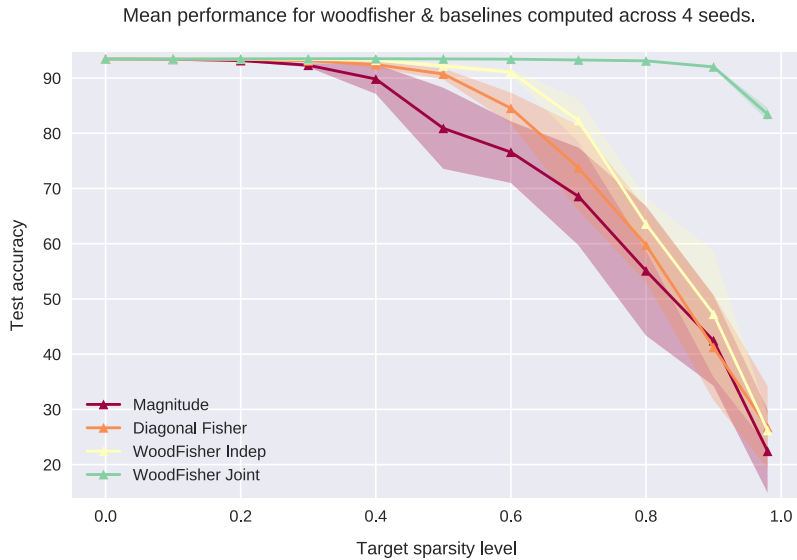


Figure 4.1 – One-shot sparsity results for MLPNET on MNIST. 8000 samples were used to estimate the empirical Fisher inverse and a dampening constant of $1e-5$ was considered.

4.1 One-shot pruning results

Here, we assume that we are given a pre-trained neural network and we would like to compress it “one-shot”. This means that we will compress the original dense network to the required size in one-go, without performing any rounds of re-training in between.

Such a scenario might actually arise in practice, where we have access to only limited amounts of training data which makes the re-training infeasible. Examples include domains where sensitive private data is involved, such as health care, legal, etc.

Further, these results will allow us to clearly distinguish which method performs better, as re-training often hides such aspects under the carpet. Also, re-training involves its own share of hyper-parameters, and an optimal setting of which might differ across methods.

4.1.1 On MNIST

As a first check, we test our method on MNIST with a small multi-layer perceptron called MLPNET, same as the one used in Section 3.1. The main baselines for this experiment are magnitude pruning (isotropic Hessian) and diagonal Fisher. Figure 4.1 presents the test accuracy results for these baselines and the WoodFisher variants at different values of sparsity. The scores in this plot have been averaged across four seeds and the standard deviation is also shown alongside.

In this experiment, we compute the full (empirical) Fisher inverse via Woodbury as the network is not that big in size. We observe that WoodFisher in the independent mode is better than

diagonal Fisher and magnitude pruning. However, we observe a high standard deviation in the results at higher sparsity values. This arises because in these three approaches all the layers are being pruned uniformly, which can result in disproportionate removal of parameters in the second and third fully-connected layers which have just 800 and 200 parameters respectively, in comparison to 31360 for the first layer. This probably causes the network to become unstable at higher pruning levels.

Whereas, if we contrast them with WoodFisher in the joint mode, we observe that WoodFisher-joint remains much more stable and maintains the same performance as the dense model up to almost 80% sparsity level. Even at 90% sparsity level, WoodFisher-joint remains in the ballpark of within 2% of the original dense model’s accuracy. Further, Table 4.1 gives some insights about the layer-wise sparsity distribution achieved by WoodFisher-joint in this high-sparsity regime.

Layer	Obtained Sparsity	Original # of params	Remaining # of params
fc1 (784 → 40)	79.7%	31,360	6,371
fc2 (40 → 20)	14.1%	800	687
fc3 (20 → 10)	6.7%	200	187

Table 4.1 – Layer-wise sparsity distribution obtained for WoodFisher-joint at 77.6% global sparsity level. The results are averaged across four seeds.

4.1.2 On CIFAR10

Now, we consider a pre-trained ResNet-20 (He et al., 2016) network on CIFAR-10. This number of parameters in this network is 272,474. So it is not possible to fit the entire Fisher inverse in a usual GPU and we resort to computing the inverse of the diagonal blocks corresponding to each layer. Figure 4.2 contains the results for one-shot pruning in this setting.

Despite the block-wise approximation, we observe that both WoodFisher-independent and WoodFisher-joint significantly outperform magnitude pruning and diagonal-Fisher based pruning. Here, we also include the global version of magnitude pruning in our comparison, given the effectiveness of pruning in this joint/global manner. We observe that the global/joint versions of magnitude pruning and WoodFisher are better than their independent counterparts.

Still, we find that the global magnitude pruning is worse than WoodFisher-independent until about 60% sparsity level, after which it is likely that having the layer-wise sparsity distribution becomes quite essential. WoodFisher-joint performs the best amongst all the methods, and is better than the top baseline of global magnitude pruning - by about 5% and 10% in test accuracy at the 70% and 80% sparsity levels.

We notice that unlike the previous results on MNIST, diagonal-Fisher performs even worse than magnitude pruning after sparsity levels higher than 30%. As a result, we do not discuss

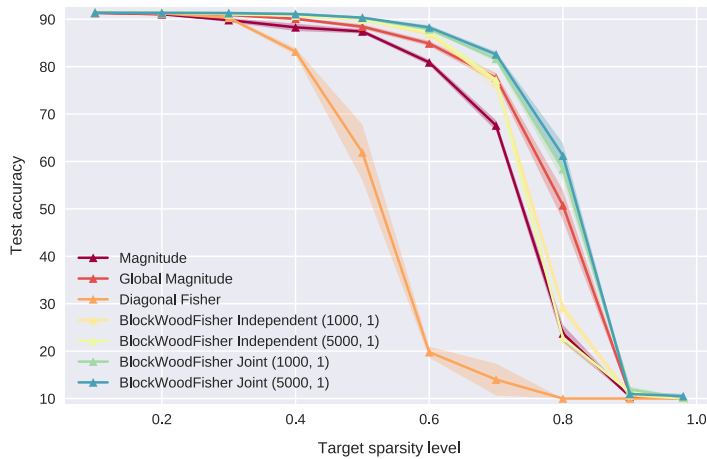


Figure 4.2 – One-shot sparsity results for ResNet-20 on CIFAR10.

its global variant in this experiment. Due to this, we will also omit its results in the sections ahead.

For the experiments on CIFAR10, we used 16,000 samples to estimate the diagonal Fisher. Whereas for WoodFisher, we find that it performs well even with 1,000 samples. Increasing the samples to 5,000 does improve the performance of WoodFisher, as observed in Figure 4.2 however this gain is mostly small. This implies that we do not need a huge number of samples to build a faithful estimate of the inverse via WoodFisher.

Overall, this highlights the importance of including the more-accurate second-order information available via WoodFisher for model pruning.

4.1.3 On ImageNet

Now, we discuss the final set of results in this series of one-shot pruning experiments. We now consider the case of ResNet-50 (which has 25,556,032 parameters) on the ImageNet dataset. This large scale setting further tests the limits of our method.

For the sake of efficiency, we further need to break the layer-wise blocks into blocks of smaller size (called ‘chunk-size’). Note, some of the layers of ResNet-50 have even more parameters than all the layers combined in the case of ResNet-20 used on CIFAR10, in the last section.

Nevertheless, in Figure 4.3, we find that using even a chunk-size of 1000 suffices to result in a strong performance gain over magnitude pruning and its global version.

Mini-batch gradient Fisher. In comparison to CIFAR-10 and MNIST, ImageNet has much more training data and output classes (1,000). Thus, in order to utilize more samples for building the estimate of the inverse via WoodFisher, we consider that each gradient in the

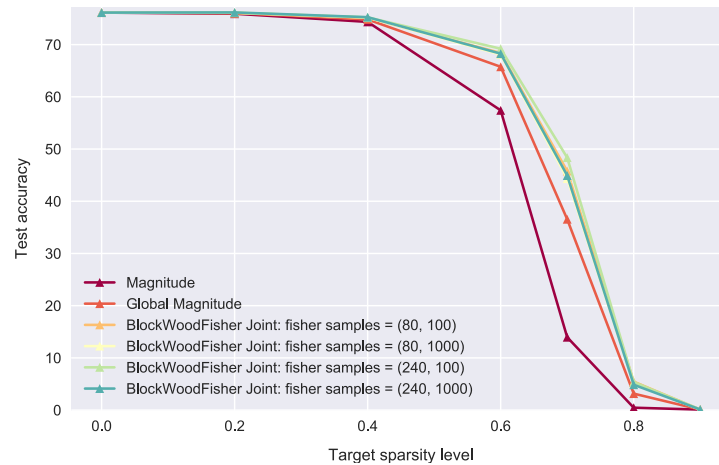
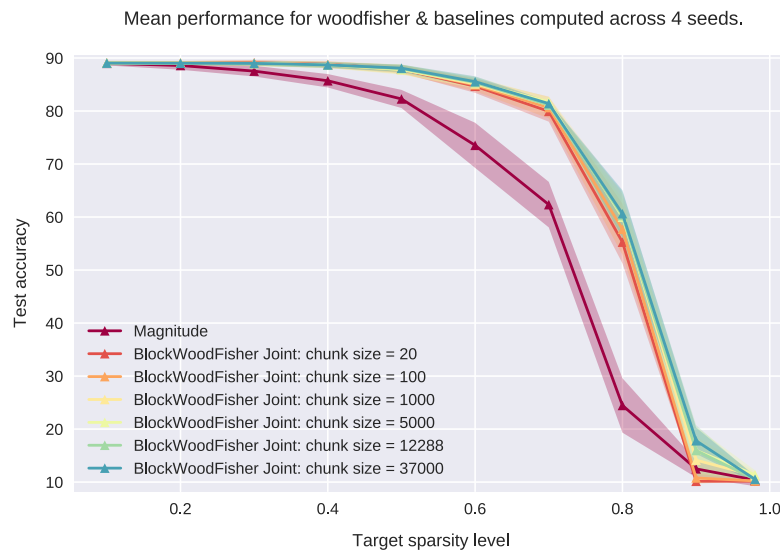


Figure 4.3 – One-shot sparsity results for ResNet-50 on ImageNet.

definition of empirical Fisher (Eqn. (1.18)) is instead averaged over a mini-batch of examples (referred to as ‘fisher-mini-bsz’). And, we find that the use of the examples in such a way to be generally helpful, without affecting the efficiency. In Figure 4.3, we show results of ‘fisher-mini-bsz’ = {100, 1000} for {80, 100} many such batches.

4.2 Ablation studies

Figure 4.4 – Effect of chunk-size on WoodFisher in the **joint** mode.

In this section, we study the effect of chunk-size (i.e., the size of blocks) on the performance of WoodFisher. We take the setting of ResNet-20 on CIFAR10. We evaluate the performance of WoodFisher for each of the chunk-sizes in the set, {20, 100, 1000, 5000, 12288, 37000}. Note that,

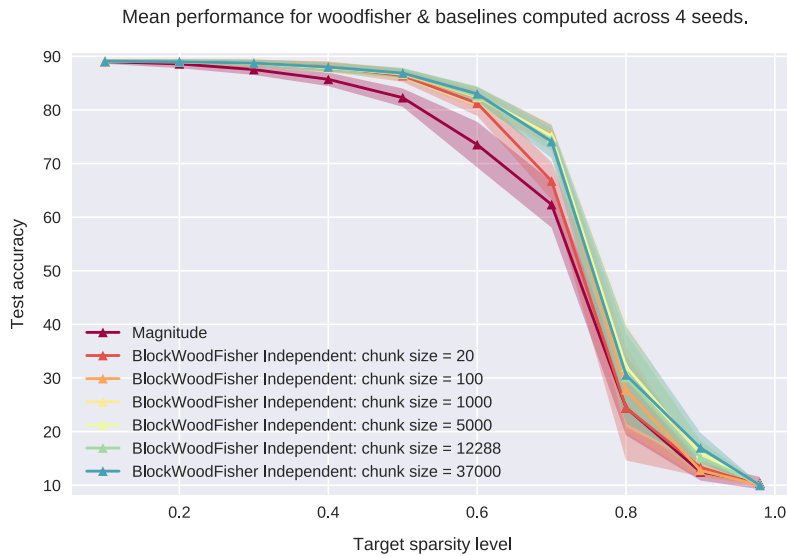


Figure 4.5 – Effect of chunk-size on WoodFisher in the **independent** mode.

37000 corresponds to the size of the block for the layer with the most number of parameters. Thus, this would correspond to taking the complete blocks across all the layers.

Figures 4.4 and 4.5 illustrate the impact of the block sizes used on the performance of WoodFisher in joint and independent mode respectively. We observe that performance of WoodFisher increases monotonically as the size of the blocks (or chunk-size) is increased, for both the cases.

This fits well with our expectation that a large chunk-size would lead to a more accurate estimation of the inverse. However, it also tells us that even starting from blocks of size as small as 100, there is a significant gain in comparison to magnitude pruning.

4.3 Gradual pruning results

It has been demonstrated in the literature (Gale et al., 2019) that gradual magnitude pruning, i.e., pruning in steps which are interspersed with re-training for a few epochs, can be very competitive to other complex approaches such as Variational Dropout (Molchanov et al., 2017) and ℓ_0 -regularization (Louizos et al., 2017).

Thus, in this section, we compare WoodFisher and magnitude pruning in this gradual pruning scenario. We follow a polynomial pruning schedule as advocated in Zhu and Gupta (2017) and prune a pre-trained ResNet-50 network on ImageNet to 80%. Figure 4.6 illustrates the obtained results in such a setting. We observe that after almost every pruning step magnitude pruning performs worse than WoodFisher.

Despite the fact such a setting with intermediate re-training allows magnitude pruning to



Figure 4.6 – Comparison of Magnitude and WoodFisher based gradual pruning of ResNet-50 on ImageNet to 80% sparsity.

recover the performance drop, it still performs worse than WoodFisher even when a large amount of fine-tuning is considered at the end. Table 4.2 shows the best results achieved by both methods. The resulting 80% sparse model obtained via WoodFisher just loses 0.05% on test accuracy in comparison to the dense model, i.e., achieving 76.08% accuracy as compared to 76.13% for the dense model.

Method	Top-1 accuracy (%)			Remaining # of params
	Dense	Pruned	Sparsity	
Magnitude	76.13	75.97	80%	5.11 M
WoodFisher	76.13	76.08	80%	5.11 M

Table 4.2 – *Best results for WoodFisher and magnitude pruning.* Both the methods follow an exactly similar schedule for gradual pruning.

To give some insights about the sparsity pattern obtained at the end via WoodFisher (in the joint mode), we plot a histogram of sparsity fractions for each of the layers in ResNet-50 in Figure 4.7. Note, how the input convolutional layers and the output fully-connected (‘fc’) layers are pruned much less (roughly half of the overall sparsity target) in comparison to some of the other layers in the middle.

This alleviates the need to define layer-wise sparsity targets or use some kind of sensitivity analysis. Also, this gives an idea of which layers are more important than others, which can find potential uses in other applications as well.

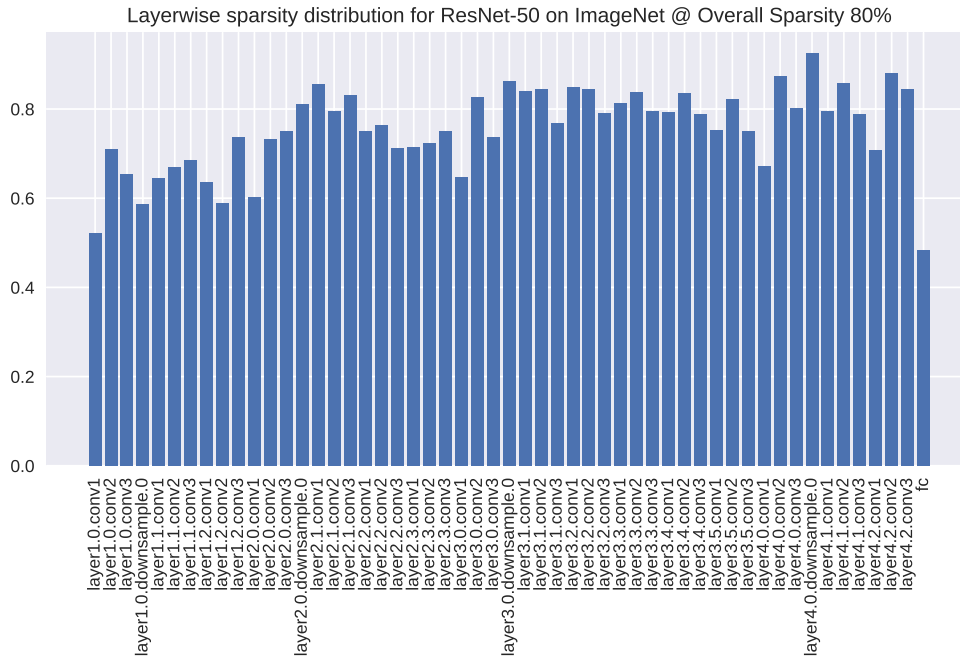


Figure 4.7 – Plot of sparsity distribution obtained by WoodFisher in joint mode when a overall target of 80% sparsity was set.

4.4 Comparison with state-of-the-art methods

In this section, we give a perspective on how the performance of WoodFisher compares with respect to the other state-of-the-art approaches for model compression.

We consider the setting of building a ResNet-50 model on ImageNet with 90% sparsity. As baselines, we consider the gradual/incremental magnitude pruning (Zhu and Gupta, 2017), as well as, dynamic pruning methods (Mostafa and Wang, 2019; Dettmers and Zettlemoyer, 2019; Lin et al., 2020).

Method	Top-1 accuracy (%)				Sparsity		Remaining
	Dense	Pruned	Difference	Relative drop	Target	Reached	# of params
Incremental (Zhu and Gupta, 2017)	75.95	73.36	-2.59	-3.41	90%	82.6%	4.45 M
DSR (Mostafa and Wang, 2019)	74.90	71.60	-3.30	-4.41	90%	80.0%	5.10 M
SM (Dettmers and Zettlemoyer, 2019)	75.95	72.65	-3.30	-4.34	90%	82.0%	4.59 M
DPF (Lin et al., 2020)	75.95	74.55	-1.44	-1.84	90%	82.6%	4.45 M
WoodFisher	76.13	75.23	-0.90	-1.18	90%	82.7%	4.42 M

Table 4.3 – Comparison of WoodFisher gradual pruning results with the state-of-the-art approaches. The numbers for the baselines are taken from Lin et al. (2020).

The important difference of dynamic pruning methods with respect to gradual pruning techniques is that the former methods perform pruning during the training. This is in comparison

4.4. Comparison with state-of-the-art methods

to the latter methods which perform the cycle of pruning and re-training once a dense model has been trained.

Note, that both kinds of methods are different approaches to compression, and are not exactly comparable. For instance, dynamic pruning methods that we compare to ahead, have the possibility to re-introduce (or re-enable) the weights which have been previously removed. This is not the case for the gradual pruning methods via WoodFisher or magnitude pruning that we consider. Similarly, gradually pruning methods can be more expensive as they require building a dense model prior to the construction of the sparse model. Nevertheless, it informs where WoodFisher stands with in comparison to other compression techniques.

We take the results in this experiment setting from a recent parallel work on dynamic pruning with error feedback (DPF; [Lin et al. \(2020\)](#)), who claim their results to be state-of-the-art. To be consistent with the baselines here, we prune all convolutional layers but do not prune the last fully-connected layer. Table 4.3 presents these results alongside with the results of our WoodFisher (joint mode). While the initial dense models used across methods are different, we compare the results in terms of the relative drop in performance for the pruned model with respect to the original dense model, so as to adjust for this.

We observe that WoodFisher¹ results in the least relative drop of performance and significantly outperforms other baseline approaches, despite requiring any re-introduction of weights. This results in a new state-of-the-art performance for constructing a 90% sparse ResNet-50 on ImageNet. Further, we would like to note that our method is in a way independent of these methods, and can be further used alongside them as a replacement of magnitude performing which is inherent to these methods.

Overall, this points to the effectiveness of using WoodFisher based pruning method which efficiently utilizes second-order information to optimally decide which parameters to prune.

¹In fact, the reported result is at 82nd epoch of the process, which was interrupted due to a system error. So it has still 8 epochs of the fine-tuning left, in comparison to baselines which use 90 epochs, and would have likely resulted in a further gain.

5 Extensions

In this chapter, we redo the analysis of compression from Section 2.2 in a more general form by factoring in the gradient term.

5.1 WoodTaylor: Pruning at a general point

Incorporating the first-order gradient term should result in a more faithful estimate for the change in loss when pruning some parameter, as many times in practice, the gradient is not exactly zero. Particularly, in the case when pruning is being carried out repeatedly or when used in dynamic pruning methods, the gradients are likely to be further away from zero. We will refer to this resulting method as ‘WoodTaylor’.

Essentially, this modifies the problem in Eq. (2.5) to as follows:

$$\min_{\delta \mathbf{w} \in \mathbb{R}^d} \left(\nabla_{\mathbf{w}} L^\top \delta \mathbf{w} + \frac{1}{2} \delta \mathbf{w}^\top \mathbf{H} \delta \mathbf{w} \right), \quad \text{s.t.} \quad \mathbf{e}_q^\top \delta \mathbf{w} + w_q = 0. \quad (5.1)$$

The corresponding Lagrangian can be then written as:

$$\mathcal{L}(\delta \mathbf{w}, \lambda) = \nabla_{\mathbf{w}} L^\top \delta \mathbf{w} + \frac{1}{2} \delta \mathbf{w}^\top \mathbf{H} \delta \mathbf{w} + \lambda \left(\mathbf{e}_q^\top \delta \mathbf{w} + w_q \right). \quad (5.2)$$

Taking the derivative of which with respect to $\delta \mathbf{w}$ yields,

$$\nabla_{\mathbf{w}} L + \mathbf{H} \delta \mathbf{w} + \lambda \mathbf{e}_q = 0 \implies \delta \mathbf{w} = -\lambda \mathbf{H}^{-1} \mathbf{e}_q - \mathbf{H}^{-1} \nabla_{\mathbf{w}} L. \quad (5.3)$$

The lagrange dual function $g(\lambda)$ can be then computed by putting the above value for $\delta \mathbf{w}$ in

the Lagrangian in Eq. (5.2) as follows:

$$\begin{aligned}
 g(\lambda) &= -\lambda \nabla_{\mathbf{w}} L^\top \mathbf{H}^{-1} \mathbf{e}_q - \nabla_{\mathbf{w}} L^\top \mathbf{H}^{-1} \nabla_{\mathbf{w}} L \\
 &+ \frac{1}{2} (\lambda \mathbf{H}^{-1} \mathbf{e}_q + \mathbf{H}^{-1} \nabla_{\mathbf{w}} L)^\top \mathbf{H} (\lambda \mathbf{H}^{-1} \mathbf{e}_q + \mathbf{H}^{-1} \nabla_{\mathbf{w}} L) \\
 &+ \lambda (-\lambda \mathbf{e}_q^\top \mathbf{H}^{-1} \mathbf{e}_q - \mathbf{e}_q^\top \mathbf{H}^{-1} \nabla_{\mathbf{w}} L + w_q) \\
 &= -\frac{\lambda^2}{2} \mathbf{e}_q^\top \mathbf{H}^{-1} \mathbf{e}_q - \lambda \mathbf{e}_q^\top \mathbf{H}^{-1} \nabla_{\mathbf{w}} L + \lambda w_q - \frac{1}{2} \nabla_{\mathbf{w}} L^\top \mathbf{H}^{-1} \nabla_{\mathbf{w}} L.
 \end{aligned} \tag{5.4}$$

As before, maximizing with respect to λ , we obtain that the optimal value λ^* of this lagrange multiplier as follows:

$$\lambda^* = \frac{w_q - \mathbf{e}_q^\top \mathbf{H}^{-1} \nabla_{\mathbf{w}} L}{\mathbf{e}_q^\top \mathbf{H}^{-1} \mathbf{e}_q} = \frac{w_q - \mathbf{e}_q^\top \mathbf{H}^{-1} \nabla_{\mathbf{w}} L}{[\mathbf{H}^{-1}]_{qq}}. \tag{5.5}$$

Note, if the gradient was 0, then we would recover the same λ^* as in Eq. (2.10). Next, the corresponding optimal perturbation, $\delta \mathbf{w}^*$, so obtained is as follows:

$$\delta \mathbf{w}^* = \frac{-(w_q - \mathbf{e}_q^\top \mathbf{H}^{-1} \nabla_{\mathbf{w}} L) \mathbf{H}^{-1} \mathbf{e}_q}{[\mathbf{H}^{-1}]_{qq}} - \mathbf{H}^{-1} \nabla_{\mathbf{w}} L. \tag{5.6}$$

In the end, the resulting change in loss corresponding to the optimal perturbation that removes parameter w_q can be written as (after some calculations¹),

$$\delta L^* = \frac{w_q^2}{2[\mathbf{H}^{-1}]_{qq}} + \frac{1}{2} \frac{(\mathbf{e}_q^\top \mathbf{H}^{-1} \nabla_{\mathbf{w}} L)^2}{[\mathbf{H}^{-1}]_{qq}} - w_q \frac{\mathbf{e}_q^\top \mathbf{H}^{-1} \nabla_{\mathbf{w}} L}{[\mathbf{H}^{-1}]_{qq}} - \frac{1}{2} \nabla_{\mathbf{w}} L^\top \mathbf{H}^{-1} \nabla_{\mathbf{w}} L. \tag{5.7}$$

Lastly, choosing the best parameter \mathbf{w}_q to be removed, corresponds to one which leads to the minimum value of the above change in loss. As in Section 2.2, our pruning statistic ρ in this setting can be similarly defined, in addition by excluding the last term in the above Eq. (5.7) since it does not involved the choice of removed parameter q . This is indicated in the Eq. (5.8) below.

$$\boxed{\rho_q = \frac{w_q^2}{2[\mathbf{H}^{-1}]_{qq}} + \frac{1}{2} \frac{(\mathbf{e}_q^\top \mathbf{H}^{-1} \nabla_{\mathbf{w}} L)^2}{[\mathbf{H}^{-1}]_{qq}} - w_q \frac{\mathbf{e}_q^\top \mathbf{H}^{-1} \nabla_{\mathbf{w}} L}{[\mathbf{H}^{-1}]_{qq}}.} \tag{5.8}$$

¹It's easier to put the optimal value of λ^* in the dual function (Eq. (5.4)) and use duality, than substituting the optimal perturbation $\delta \mathbf{w}^*$ in the primal objective.

5.2 Empirical Results

5.2.1 Partially trained model

First, we present the results for the case when the model is far from the optimum, and hence the gradient is not close to zero. This setting will allow us to clearly see the effect of incorporating the first-order gradient term, considered in the WoodTaylor analysis. In particular, we consider an MLPNET on MNIST, which has only been trained for 2 epochs. This setup is identical to that in Section 4.1.1, except that the setting in the previous chapter was aimed at compressing models at (or close to) convergence.

Figure 5.1 presents the results² for performing one-shot compression for various sparsity levels at this stage in the training. Similar to the observations in Section 4.1.1, we find that WoodFisher (joint mode) is better than magnitude or diagonal Fisher based pruning. But the more interesting aspect is the significant improvement brought about by WoodTaylor. In fact, compressing the model via WoodTaylor improves test accuracy by about 5% over the accuracy of the initial dense model, up to sparsity levels of 80%.

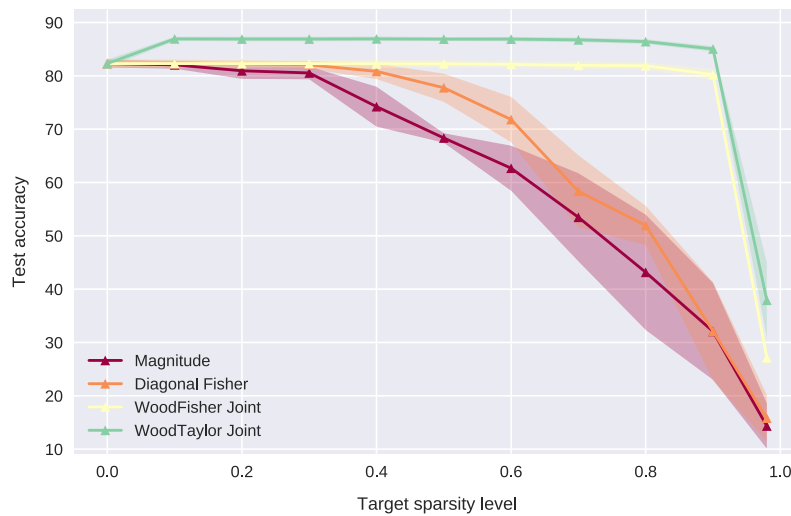


Figure 5.1 – Comparing one-shot sparsity results for WoodTaylor and WoodFisher on the partially trained MLPNET on CIFAR-10.

This points towards the potential benefit of using WoodTaylor in the dynamic pruning scenario, like along with [Lin et al. \(2020\)](#). Further, we show ahead that this benefit (albeit smaller relative to here) can be observed even in the pre-trained setting, where the gradient is close to zero.

²Here, the number of samples used for Fisher in both WoodTaylor and WoodFisher is 8000. A dampening of $1e-1$ was used for WoodTaylor, while WoodFisher is insensitive to dampening as discussed in the next section.

5.2.2 Pre-trained model

Next, we focus on the comparison between WoodFisher and WoodTaylor for the setting of ResNet-20 pre-trained on CIFAR10, where both the methods are used in their ‘full-matrix’ mode. In other words, no block-wise assumption is made, and we consider pruning only the ‘layer1.0.conv1’, ‘layer1.0.conv2’ and ‘layer2.0.conv1’. In Figure 5.2, we present the results of one-shot experiments in this setting.

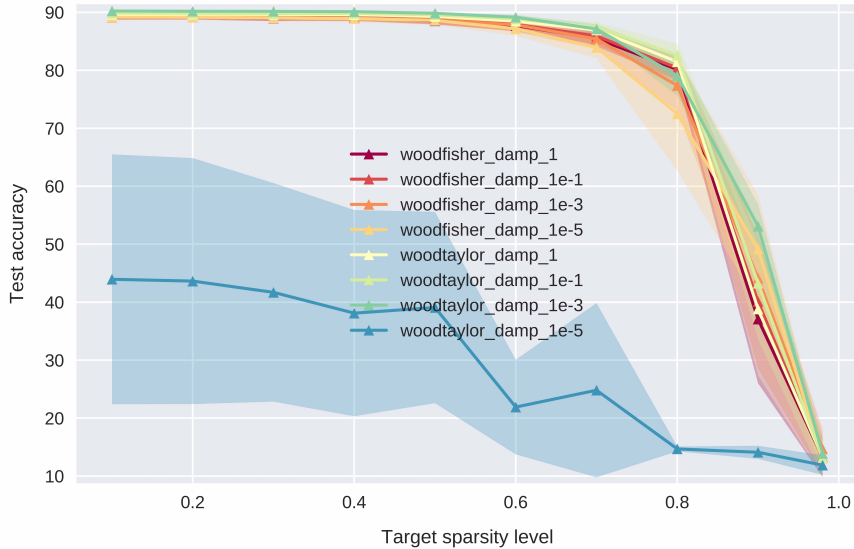


Figure 5.2 – Comparing one-shot sparsity results for WoodTaylor and WoodFisher on CIFAR-10 for ResNet-20.

We observe that WoodTaylor (with $damp=1e-3$) outperforms WoodFisher (across various dampening values) for almost all levels of target sparsity. This confirms our hypothesis of factoring in the gradient term, which even in this case where the model has relatively high accuracy, can lead to a gain in performance. However, it is important to that in comparison to WoodFisher, WoodTaylor is more sensitive to the choice of hyper-parameters like the dampening value, as reflected in the Figure 5.2. This arises because now in the weight update, Eqn. (5.6), there are interactions between the Hessian inverse and gradient terms, due to which the scaling of the inverse Hessian governed by this dampening becomes more important. To give an example, in the case where $damp=1e-5$, the resulting weight update has about $10\times$ bigger norm than that of the original weight.

This can be easily adjusted via the dampening, but unlike WoodFisher, it is not hyper-parameter free. Also, for these experiments, the number of samples used was 50,000, which is higher in comparison to our previously used values. In order to better understand the sensitivity of WoodTaylor with respect to these hyper-parameter choices, we present an ablation study in Figure 5.3 that measures their effect on WoodTaylor’s performance.

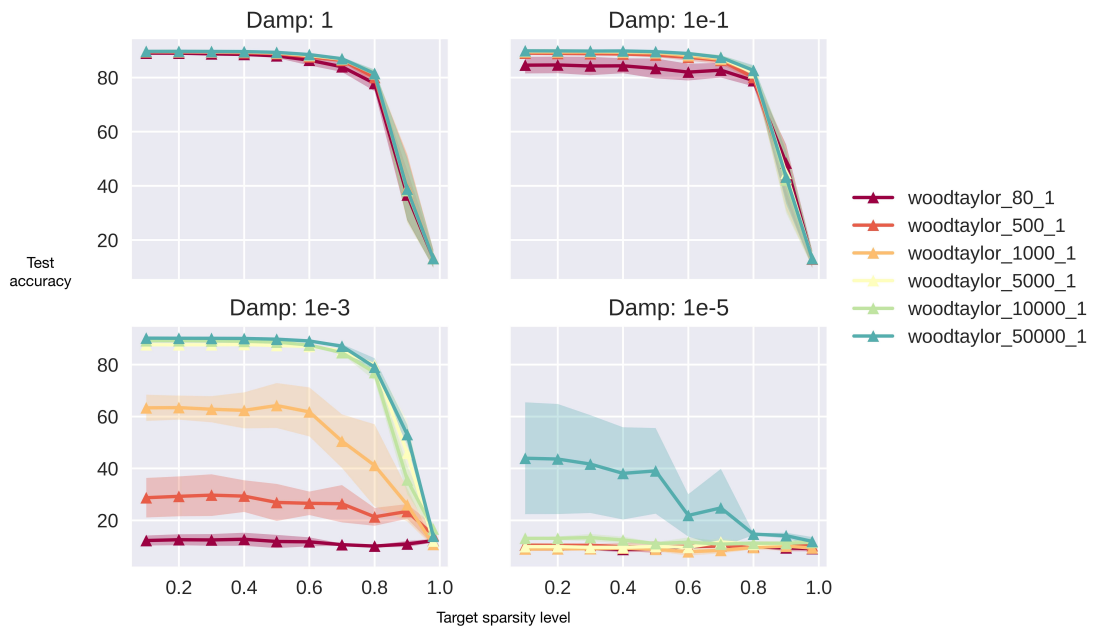


Figure 5.3 – Ablation study for WoodTaylor that shows the effect of dampening and the number of samples used on the performance.

In the end, we conclude that incorporating the first-order term helps WoodTaylor to gain in performance over WoodFisher, however, some hyper-parameter tuning for the dampening constant might be required. Future work would aim to apply WoodTaylor in the setting of gradual pruning discussed in Chapter 4.

6 Conclusion and Future Work

In this work, we have shown how our method *WoodFisher*, in the form of empirical Fisher matrix used along with the Woodbury matrix identity, can serve as an efficient yet accurate local quadratic model for deep neural networks which have dimensions in the orders of millions. When applied to the task of model compression in the framework of Optimal Brain Damage/Surgeon (LeCun et al., 1990; Hassibi and Stork, 1993), this results in a state-of-the-art one-shot pruner, as well as performs at par or better than dynamic and gradual pruning methods.

Nevertheless, there are several exciting avenues which we could not address in this work:

- **One-shot pruning with intermediate local quadratic model updates:** For instance, in the case of model compression, we would ideally like to update our estimate of the Hessian approximation after certain amounts of pruning, since the underlying Taylor-series approximation holds only in a local neighbourhood. Despite this fact, in our one-shot experiments, we were able to prune up to the levels of 60% sparsity without losing much in performance. However, it is evident that refining our local quadratic model after every few steps can lead to a further improvement in performance, especially for even higher sparsity levels.
- **Refining the local quadratic model with cubic-regularization:** Another way in which we can further improve our local quadratic model is by taking into account the ignored third-order term. This can possibly be achieved by introducing a cubic regularization term in the local model (Nesterov and Polyak, 2006).
- **Efficient preconditioner for optimization:** Equipped with an efficient method to estimate inverse Hessian-vector products (IHVPs), it is natural to consider the application of *WoodFisher* as a preconditioner in optimization. The added advantage of *WoodFisher* in the case of optimization is that the gradients needed to compute the IHVP are available for free during the usual training procedure.
- **Other applications:** It would be relevant to consider other applications where efficient

Chapter 6. Conclusion and Future Work

IHVPs are required, like influence-functions ([Koh and Liang, 2017](#)), as well as areas where better one-shot pruners can be employed, such as finding lottery tickets ([Frankle and Carbin, 2018](#)).

Bibliography

- Agarwal, N., Bullins, B., and Hazan, E. (2016). Second-order stochastic optimization for machine learning in linear time.
- Amari, S.-i. (1998). Natural gradient works efficiently in learning. *Neural Computation*, 10(2):251–276.
- Ba, J., Grosse, R., and Martens, J. (2016). Distributed second-order optimization using kronecker-factored approximations.
- Carreira-Perpinán, M. A. and Idelbayev, Y. (2018). “learning-compression” algorithms for neural net pruning. In *Proceedings of the IEEE Conference on Computer Vision and Pattern Recognition*, pages 8532–8541.
- Chen, W., Wilson, J. T., Tyree, S., Weinberger, K. Q., and Chen, Y. (2015). Compressing neural networks with the hashing trick. In *ICML*.
- Cheng, Y., Wang, D., Zhou, P., and Zhang, T. (2017). A survey of model compression and acceleration for deep neural networks.
- Chou, Y.-M., Chan, Y.-M., Lee, J.-H., Chiu, C.-Y., and Chen, C.-S. (2018). Unifying and merging well-trained deep neural networks for inference stage. *arXiv preprint arXiv:1805.04980*.
- Dettmers, T. and Zettlemoyer, L. (2019). Sparse networks from scratch: Faster training without losing performance.
- Devlin, J., Chang, M.-W., Lee, K., and Toutanova, K. (2018). Bert: Pre-training of deep bidirectional transformers for language understanding.
- Dong, X., Chen, S., and Pan, S. J. (2017). Learning to prune deep neural networks via layer-wise optimal brain surgeon.
- Duchi, J. C., Hazan, E., and Singer, Y. (2010). Adaptive subgradient methods for online learning and stochastic optimization. *J. Mach. Learn. Res.*, 12:2121–2159.
- Frankle, J. and Carbin, M. (2018). The lottery ticket hypothesis: Finding sparse, trainable neural networks.

Bibliography

- Gale, T., Elsen, E., and Hooker, S. (2019). The state of sparsity in deep neural networks.
- Grosse, R. and Martens, J. (2016). A kronecker-factored approximate fisher matrix for convolution layers.
- Guo, Y., Yao, A., and Chen, Y. (2016). Dynamic network surgery for efficient dnns.
- Han, S., Mao, H., and Dally, W. J. (2015). Deep compression: Compressing deep neural networks with pruning, trained quantization and huffman coding.
- Hassibi, B. and Stork, D. G. (1993). Second order derivatives for network pruning: Optimal brain surgeon. In Hanson, S. J., Cowan, J. D., and Giles, C. L., editors, *Advances in Neural Information Processing Systems 5*, pages 164–171. Morgan-Kaufmann.
- He, K., Zhang, X., Ren, S., and Sun, J. (2016). Deep residual learning for image recognition. *2016 IEEE Conference on Computer Vision and Pattern Recognition (CVPR)*.
- Heskes, T. (2000). On natural learning and pruning in multilayered perceptrons. *Neural Computation*, 12:881–901.
- Hinton, G., Vinyals, O., and Dean, J. (2015). Distilling the knowledge in a neural network.
- Kingma, D. P. and Ba, J. (2014). Adam: A method for stochastic optimization.
- Koh, P. W. and Liang, P. (2017). Understanding black-box predictions via influence functions.
- Krishnan, S., Xiao, Y., and Saurous, R. A. (2018). Neumann optimizer: A practical optimization algorithm for deep neural networks. In *International Conference on Learning Representations*.
- Kunstner, F., Balles, L., and Hennig, P. (2019). Limitations of the empirical fisher approximation for natural gradient descent.
- Laurent, C., George, T., Bouthillier, X., Ballas, N., and Vincent, P. (2018). An evaluation of fisher approximations beyond kronecker factorization.
- LeCun, Y., Bengio, Y., and Hinton, G. (2015). Deep learning. *nature*, 521(7553):436–444.
- LeCun, Y., Denker, J. S., and Solla, S. A. (1990). Optimal brain damage. In Touretzky, D. S., editor, *Advances in Neural Information Processing Systems 2*, pages 598–605. Morgan-Kaufmann.
- Li, H., Kadav, A., Durdanovic, I., Samet, H., and Graf, H. P. (2016). Pruning filters for efficient convnets. *ArXiv*, abs/1608.08710.
- Lin, T., Stich, S. U., Barba, L., Dmitriev, D., and Jaggi, M. (2020). Dynamic model pruning with feedback. In *International Conference on Learning Representations*.
- Louizos, C., Welling, M., and Kingma, D. P. (2017). Learning sparse neural networks through l_0 regularization.

- Luo, J.-H., Wu, J., and Lin, W. (2017). Thinet: A filter level pruning method for deep neural network compression. *2017 IEEE International Conference on Computer Vision (ICCV)*.
- Martens, J. (2010). Deep learning via hessian-free optimization. In *Proceedings of the 27th International Conference on International Conference on Machine Learning, ICML'10*, page 735–742, Madison, WI, USA. Omnipress.
- Martens, J. (2014). New insights and perspectives on the natural gradient method.
- Martens, J., Ba, J., and Johnson, M. (2018). Kronecker-factored curvature approximations for recurrent neural networks. In *International Conference on Learning Representations*.
- Martens, J. and Grosse, R. (2015). Optimizing neural networks with kronecker-factored approximate curvature.
- Molchanov, D., Ashukha, A., and Vetrov, D. (2017). Variational dropout sparsifies deep neural networks.
- Mostafa, H. and Wang, X. (2019). Parameter efficient training of deep convolutional neural networks by dynamic sparse reparameterization.
- Mozer, M. C. and Smolensky, P. (1989). Skeletonization: A technique for trimming the fat from a network via relevance assessment. In *Advances in neural information processing systems*, pages 107–115.
- Nesterov, Y. and Polyak, B. T. (2006). Cubic regularization of newton method and its global performance. *Mathematical Programming*, 108(1):177–205.
- Osawa, K., Tsuji, Y., Ueno, Y., Naruse, A., Yokota, R., and Matsuoka, S. (2019). Large-scale distributed second-order optimization using kronecker-factored approximate curvature for deep convolutional neural networks. *2019 IEEE/CVF Conference on Computer Vision and Pattern Recognition (CVPR)*.
- Pearlmutter, B. A. (1994). Fast exact multiplication by the hessian. *Neural Comput.*, 6(1):147–160.
- Radford, A. (2018). Improving language understanding by generative pre-training.
- Rajbhandari, S., Rasley, J., Ruwase, O., and He, Y. (2019). Zero: Memory optimization towards training a trillion parameter models. ArXiv.
- Ren, S., He, K., Girshick, R., and Sun, J. (2015). Faster r-cnn: Towards real-time object detection with region proposal networks. In Cortes, C., Lawrence, N. D., Lee, D. D., Sugiyama, M., and Garnett, R., editors, *Advances in Neural Information Processing Systems 28*, pages 91–99. Curran Associates, Inc.
- Sagun, L., Evci, U., Guney, V. U., Dauphin, Y., and Bottou, L. (2018). Empirical analysis of the hessian of over-parametrized neural networks.

Bibliography

- Schmidhuber, J. (2015). Deep learning in neural networks: An overview. *Neural networks*, 61:85–117.
- Schraudolph, N. N. (2002). Fast curvature matrix-vector products for second-order gradient descent. *Neural Computation*, 14(7):1723–1738.
- Singh, S. P. and Jaggi, M. (2019). Model fusion via optimal transport.
- Theis, L., Korshunova, I., Tejani, A., and Huszár, F. (2018). Faster gaze prediction with dense networks and fisher pruning.
- Wang, C., Grosse, R., Fidler, S., and Zhang, G. (2019). Eigendamage: Structured pruning in the kronecker-factored eigenbasis.
- Wu, Y., Mansimov, E., Grosse, R. B., Liao, S., and Ba, J. (2017). Second-order optimization for deep reinforcement learning using kronecker-factored approximation. In *NIPS*, pages 5285–5294.
- Zeng, W. and Urtasun, R. (2019). MLPrune: Multi-layer pruning for automated neural network compression.
- Zhu, M. and Gupta, S. (2017). To prune, or not to prune: exploring the efficacy of pruning for model compression.